The first six months of the Advanced LIGO's and Advanced Virgo's third observing run with GRANDMA

S. Antier, S. Agayeva, V. Aivazyan, S. Alishov, E. Arbouch, A. Baransky, K. Barynova, J.M. Bai, S. Basa, S. Beradze, et al.

Monthly Notices
of the
ROYAL ASTRONOMICAL SOCIETY

MNRAS **492,** 3904–3927 (2020)
Advance Access publication 2019 November 11

doi:10.1093/mnras/stz3142

The first six months of the Advanced LIGO's and Advanced Virgo's third observing run with GRANDMA

S. Antier[1★] S. Agayeva,[2] V. Aivazyan,[3,4] S. Alishov,[2] E. Arbouch,[5] A. Baransky,[6] K. Barynova,[7] J. M. Bai,[8] S. Basa,[9] S. Beradze,[3,4] E. Bertin,[5] J. Berthier,[10] M. Blažek,[11] M. Boër,[12] O. Burkhonov,[13] A. Burrell,[14] A. Cailleau,[15] B. Chabert,[14,16] J. C. Chen,[17] N. Christensen,[12] A. Coleiro,[1] B. Cordier,[18] D. Corre,[19] M. W. Coughlin,[20] D. Coward,[14] H. Crisp,[14] C. Delattre,[10] T. Dietrich,[21] J.-G. Ducoin,[19] P.-A. Duverne,[19] G. Marchal-Duval,[19] B. Gendre,[14] L. Eymar,[12] P. Fock-Hang,[10] X. Han,[22] P. Hello,[19] E. J. Howell,[14] R. Inasaridze,[3,4] N. Ismailov,[2] D. A. Kann,[11] G. Kapanadze,[3,4] A. Klotz,[15,16] N. Kochiashvili,[3] C. Lachaud,[1] N. Leroy,[19] A. Le Van Su,[9] W. L. Lin,[23] W. X. Li,[23] P. Lognone,[19] R. Marron,[1] J. Mo,[23] J. Moore,[14] R. Natsvlishvili,[3] K. Noysena,[12,15] S. Perrigault,[10] A. Peyrot,[10] D. Samadov,[2] T. Sadibekova,[13,18] A. Simon,[24] C. Stachie,[12] J. P. Teng,[10] P. Thierry,[10] C. C. Thöne,[11] Y. Tillayev,[13] D. Turpin,[22] A. de Ugarte Postigo,[11] F. Vachier,[10] M. Vardosanidze,[3,4] V. Vasylenko,[24] Z. Vidadi,[2] X. F. Wang,[23] C. J. Wang,[8] J. Wei,[22] S. Y. Yan,[23] J. C. Zhang,[23] J. J. Zhang[8] and X. H. Zhang[23]

Affiliations are listed at the end of the paper

Accepted 2019 October 31. Received 2019 October 28; in original form 2019 July 10

ABSTRACT

We present the Global Rapid Advanced Network Devoted to the Multi-messenger Addicts (GRANDMA). The network consists of 21 telescopes with both photometric and spectroscopic facilities. They are connected together thanks to a dedicated infrastructure. The network aims at coordinating the observations of large sky position estimates of transient events to enhance their follow-up and reduce the delay between the initial detection and optical confirmation. The GRANDMA programme mainly focuses on follow-up of gravitational-wave alerts to find and characterize the electromagnetic counterpart during the third observational campaign of the Advanced LIGO and Advanced Virgo detectors. But it allows for follow-up of any transient alerts involving neutrinos or gamma-ray bursts, even those with poor spatial localization. We present the different facilities, tools, and methods we developed for this network and show its efficiency using observations of LIGO/Virgo S190425z, a binary neutron star merger candidate. We furthermore report on all GRANDMA follow-up observations performed during the first six months of the LIGO–Virgo observational campaign, and we derive constraints on the kilonova properties assuming that the events' locations were imaged by our telescopes.

Key words: gravitational waves – methods: observational – stars: neutron.

1 INTRODUCTION

The first gravitational wave (GW) observation of a coalescing binary neutron star (BNS), GW170817, by the Advanced LIGO (Aasi et al. 2015) and Advanced Virgo (Acernese et al. 2015) (aLIGO/Virgo) detectors and the prompt joint observations by *Fermi*-GBM (Gamma-ray burst monitor) and *INTEGRAL* of the short-duration gamma-ray burst (sGRB) 170817A (Abbott et al. 2017d; Goldstein et al. 2017; Savchenko et al. 2017) established the association between sGRBs and BNS mergers (Eichler et al. 1989). The localization to within 28 deg^2, together with a lumi-

★ E-mail: antier@apc.in2p3.fr

nosity distance measured by the GW signal of 40 Mpc (Abbott et al. 2017a), prompted a groundbreaking electromagnetic (EM) follow-up campaign that initiated the era of GW multimessenger astronomy (Abbott et al. 2017c). The independent observation of the macronova/kilonova (KN) of GW170817 (Abbott et al. 2017c; Andreoni et al. 2017; Hallinan et al. 2017; Kasliwal et al. 2017; Troja et al. 2017) and its spectral evolution from blue to red helped to understand the merger process and allowed an identification of the host galaxy. The agreement between theoretical kilonova predictions (see Metzger 2017 and references therein) and the observational data revealed that BNS mergers are an important aspect of the production of heavy elements (see e.g. Just et al. 2015; Kasliwal et al. 2019a). In addition, the joint GW/EM observation allowed a new measurement of the expansion rate of the universe (Abbott et al. 2017b; Hotokezaka et al. 2019), it conclusively showed BNS mergers can be engines for sGRBs (Abbott et al. 2017c), it placed precise limits on the propagation speed of GWs (Abbott et al. 2017c), it ruled out a number of alternative theories of gravity (see e.g. Baker et al. 2017; Creminelli & Vernizzi 2017; Ezquiaga & Zumalacarregui 2017), and it placed new constraints on the equation of state of cold supranuclear matter (see e.g. Bauswein, Baumgarte & Janka 2013; Abbott et al. 2017a; Coughlin et al. 2018b; Radice et al. 2018; Capano et al. 2019; Coughlin et al. 2019b; Radice & Dai 2019). Late-time observations from X-rays to the radio bands monitored the afterglow (Lyman et al. 2018; Margutti et al. 2018; Resmi et al. 2018; Ruan et al. 2018; Troja et al. 2018a; Fong et al. 2019) before eventually showing that a successful jet was launched and that the early non-kilonova emission might be from a structured jet viewed 20°–30° from the jet axis (Mooley et al. 2018; Troja et al. 2018b; Ghirlanda et al. 2019; Howell et al. 2019a).

Despite all these advances and the general consistency between predictions and observational data, a number of things are still unknown. Most notably, there are a number of different kilonova models, (see e.g. Metzger 2019 and references therein) that explain the observational data well but predict different light-curve evolutions for the first hours after the merger of the two compact objects (Arcavi 2018). Thus, an early-time observation within the first few hours of a merger might provide important additional information about the fast ejecta components, the composition of the ejected material, and the heating rate for the unbound material. Early-time data could also rule out other contribution channels or kilonova pre-cursors powered by free neutron decay (Metzger et al. 2015).

The third aLIGO/Virgo observing run (O3), which started in 2019 April, is now underway with expected BNS detection rates of between 1 and 16 events a year (Howell et al. 2019a) and the number of triggers for binary black hole (BBH) mergers being sent out as GW alerts of order 1 per week[1] and a reasonable chance of detecting the first black hole–neutron star merger (Pannarale & Ohme 2014; Bhattacharya, Kumar & Smoot 2019). With the increased detection ranges[2] and thus increased detection rates comes an intense effort to observe and monitor any EM counterparts. This task is very challenging and as experienced during the second observing run (The LIGO Scientific Collaboration & the Virgo Collaboration 2019), surveying sky areas of the order of 100–1000 s of square degrees requires an important coordinated effort between telescopes spread across different locations on Earth.

A worldwide network is thus required to optimize the EM follow-up of GW events. For this purpose, the Global Rapid Advanced Network Devoted to the Multi-messenger Addicts (GRANDMA) was created in 2018 April, reusing existing facilities built in the 1960s and 1970s as well as newer robotic telescope systems. The aim of this paper is to present this collaboration and its network of telescopes. We list the components of the network in Section 2. The observational strategy and the full GRANDMA system is presented in Section 3. In Section 4, we present statistics on all GRANDMA follow-up observations obtained during the first six months of the LIGO–Virgo observing run O3, up until the one-month pause in 2019 October. We present the GRANDMA follow-up of the S190425z alert to illustrate the versatility of the programme, from the rapid scanning of the GW sky localization area to the analysis of the counterpart candidates. We also derive constraints on the kilonova properties assuming that the events' locations were imaged by our telescopes for S190425z, the closest alert from the first half of the run. In the concluding section, we discuss possible improvements to telescope networks to face new challenges presented by time-domain astronomy.

2 GRANDMA CONSORTIUM

2.1 A network for GW follow-up of transients with large localization uncertainties

GRANDMA is a worldwide network of 21 telescopes with both photometric and spectroscopic facilities, with a large amount of time allocated for observing transient alerts as a telescope network (see Fig. 1, Table 1, and Table 2). The GRANDMA consortium includes 15 observatories, 24 institutions, and groups from nine countries. Most of the allocated time available to GRANDMA is proprietary, i.e. warranted recurring time. Because of that, and the large amount of observing time, the collaboration can cover thousands of square degrees within 24 h, which allows for a rapid scan of the sky localization area of any GW alert triggered during aLIGO/Virgo O3. In this sense, GRANDMA has the capacity to catch the early stage of the visible components of the post-merger ejected material with rapid online colour identification. While GRANDMA has some shortcomings in performing very deep spectroscopic follow-ups that require large telescopes (for example 4 m class telescopes), it offers unique worldwide observational capabilities complementary to those of other collaborations.

The GRANDMA network has access to four wide-field telescopes (field of view [FoV] $> 1\,\mathrm{deg}^2$) located on three continents, with the TAROT network (≈18 mag in 60 s) (Klotz et al. 2008; Noysena et al. 2019) and the OAJ-T80 telescope (≈21 mag in 180 s). GRANDMA also has access to 10 remote and robotic telescopes with narrower FoVs, reaching at a minimum a limiting magnitude of 18. The two groups of telescopes are used to rapidly find counterpart candidates, either tiling the localization area of the GW alerts or targeting host-galaxy candidates. These 14 telescopes can use the full available night to observe GW sky localization areas, depending only on weather conditions. The remaining telescopes of the collaboration are used to confirm an association and to perform dedicated follow-up observations, either photometrically or spectroscopically.

The prompt full coverage of the transient sky accessible by GRANDMA at a given time is presented in Fig. 2. In 24 h,

[1] See https://www.gw-openscience.org/alerts/

[2] At the time of writing, the detection ranges for average orientated and located BNSs have reached around 140, 120, and 50 Mpc for LIGO-Livingston, LIGO-Hanford, and Virgo, respectively; see https://www.gw-openscience.org/detector_status/ for the current status of the instruments.

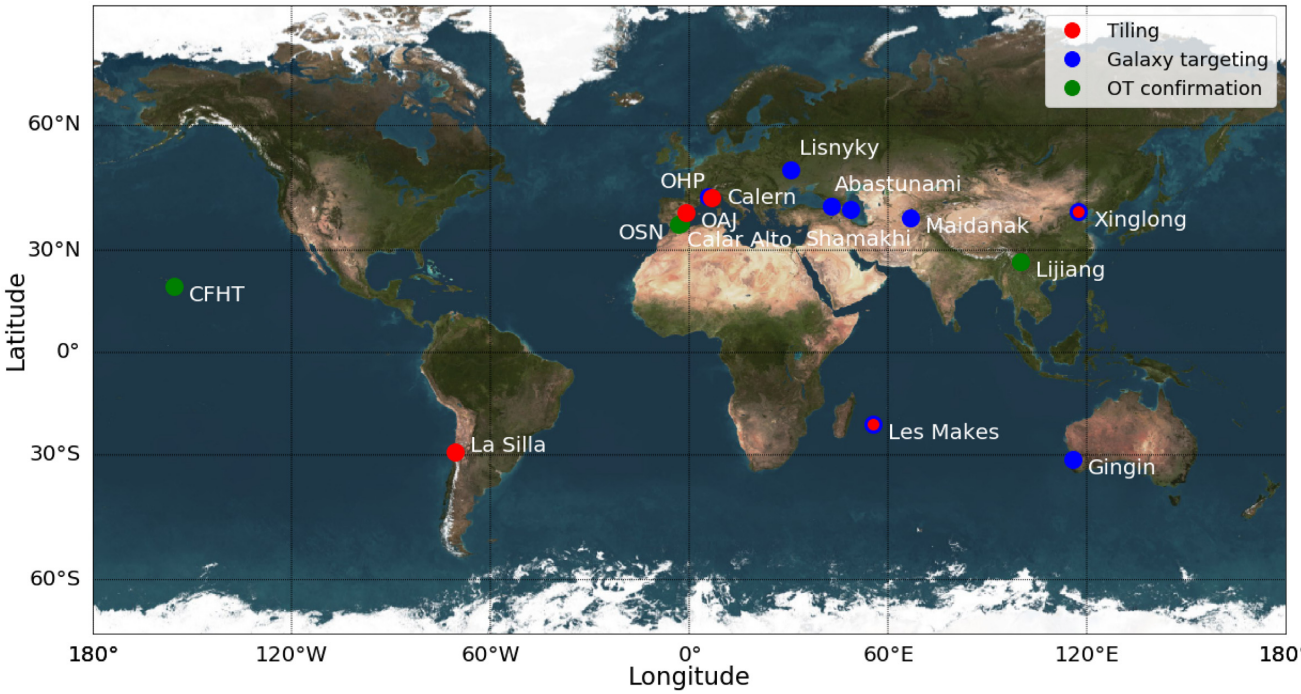

Figure 1. Locations of the 15 observatories involved in the GRANDMA network. The colour encodes the observation strategy followed by telescopes at a given observatory: *red* for tiling, *blue* for targeting galaxies, *green* for following up candidates.

Table 1. List of telescopes of the GRANDMA consortium and their photometric performance when using their standard setup.

Telescope name	Location	Aperture (m)	FoV (deg)	Filters	$3-\sigma$ limit (AB mag)	Maximum night slot (UTC) (h)
TAROT/TCH	La Silla Obs.	0.25	1.85 × 1.85	Clear, $g'r'i'$	18.0 in 60 s (Cear)	06–15
CFHT/WIRCAM	CFH Obs.	3.6	0.35 × 0.35	JH	22.0 in 200 s (J)	10–16
CFHT/MEGACAM	CFH Obs.	3.6	1.0 × 1.0	$g'r'i'z'$	23.0 in 200 s (r')	10–16
Zadko	Gingin Obs.	1.00	0.17 × 0.12	Clear, $g'r'i'I_C$	20.5 in 40 s (Clear)	12–22
TNT	Xinglong Obs.	0.80	0.19 × 0.19	$BVg'r'i'$	19.0 in 300 s (R_C)	12–22
Xinglong-2.16	Xinglong Obs.	2.16	0.15 × 0.15	$BVRI$	21.0 in 100 s (R_C)	12–22
GMG-2.4	Lijiang Obs.	2.4	0.17 × 0.17	$BVRI$	22.0 in 100 s (R_C)	12–22
UBAI/NT-60	Maidanak Obs.	0.60	0.18 × 0.18	BVR_CI_C	18.0 in 180 s (R_C)	14–00
UBAI/ST-60	Maidanak Obs.	0.60	0.11 × 0.11	BVR_CI_C	18.0 in 180 s (R_C)	14–00
TAROT/TRE	La Reunion	0.18	4.2 × 4.2	Clear	16.0 in 60 s (Clear)	15–01
Les Makes/T60	La Reunion.	0.60	0.3 × 0.3	Clear, BVR_C	19.0 in 180 s (R_C)	15–01
Abastumani/T70	Abastumani Obs.	0.70	0.5 × 0.5	BVR_CI_C	18.2 in 60 s (R_C)	17–03
Abastumani/T48	Abastumani Obs.	0.48	0.33 × 0.33	$UBVR_CI_C$	15.0 in 60 s (R_C)	17–03
ShAO/T60	Shamakhy Obs.	0.60	0.28 × 0.28	BVR_CI_C	19.0 in 300 s (R_C)	17–03
Lisnyky/AZT-8	Kyiv Obs.	0.70	0.38 × 0.38	$UBVR_CI_C$	20.0 in 300 s(R_C)	17–03
TAROT/TCA	Calern Obs.	0.25	1.85 × 1.85	Clear, $g'r'i'$	18.0 in 60 s (Clear)	20–06
IRIS	OHP	0.5	0.4 × 0.4	Clear,$u'g'r'i'z'$	18.5 in 60 s (r')	20–06
T120	OHP	1.20	0.3 × 0.3	$BVRI$	20.0 in 60 s (R)	20–06
OAJ/T80	Javalambre Obs.	0.80	1.4 × 1.4	r'	21.0 in 180 s (r')	20–06
OSN/T150	Sierra Nevada Obs.	1.50	0.30 × 0.22	BVR_CI_C	21.5 in 180 s (R_C)	20–06
CAHA/2.2m	Calar Alto Obs.	2.20	0.27⌀	$u'g'r'i'z'$	23.7 in 100 s (r')	20–06

Table 2. List of telescopes of the GRANDMA consortium with spectroscopic capabilities.

Telescope/Instrument	Location	Wavelength range	Spectral resolution $\lambda/\Delta\lambda$	Limiting mag
2.2m CAHA/CAFOS	Calar Alto Obs.	3200–7000/6300–11 000	400	20 in 1h
ShAO/T2m	Shamakhy Obs.	3800–7000	2000	17 in 1h
Xinglong-2.16/BFOSC	Xinglong Obs.	3600–9600	1000	18 in 1h
GMG-2.4/YFOSC	Lijiang Obs.	3400–9100	2000	19 in 1h

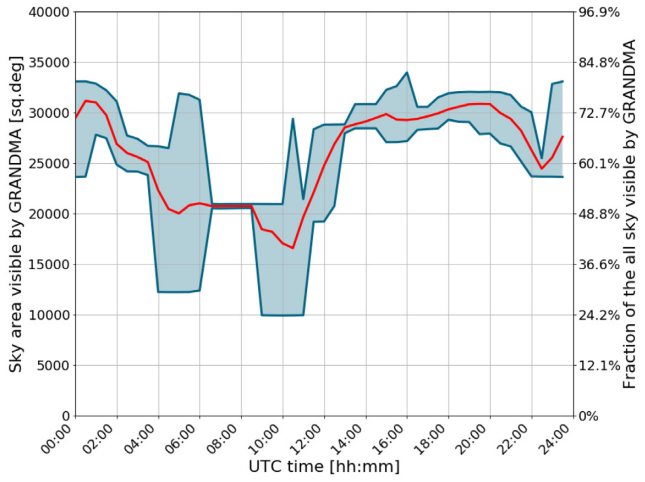

Figure 2. The sky area visible during local nighttime (in square degrees and in percentage) to the GRANDMA network (15 observatories) as a function of time during a day. The red line represents the daily sky coverage averaged over a year while the blue area gives the minimum and maximum sky coverage reachable during a year. The visibility gap between 04:00 and 12:00 is due to the lack of observatories at western longitudes.

thanks to an extensive distribution on Earth and especially at eastern longitudes, the GRANDMA network is able to access over 60 per cent of the sky (up to more than 72 per cent) during nights[3] to a limiting magnitude of 18 mag about 75 per cent of the time. Due to a lack of western observatories, the sky coverage is reduced to 40–50 per cent during the western nights. All the telescopes are connected to the ICARE (*Interface and Communication for Addicts of the Rapid follow-up in multi-messenger Era*), which automatically provides dedicated observation plans to any telescope (described in Section 3) as soon as a GW alert is received. Finally, in the case of a confident detection of an EW counterpart to a GW event, GRANDMA has access to four 2m-class telescopes in three different time zones with photometric depth capabilities of ≈22 mag and spectroscopic depth capabilities of ≈18.5 mag, as shown in Table 2. All the results of the observations and counterpart candidates are centralized in a unique data base to optimize the follow-up and repoint telescopes to counterpart candidates.

Since the beginning of 2019 April and until the one-month pause in 2019 October, GRANDMA had already responded to 27/33 alerts sent by the LIGO–Virgo collaboration (see Section 4), making it one of the most active networks following up GW alerts. Presented below are descriptions of the telescopes participating in the GRANDMA network.

2.2 Abastumani Astrophysical Observatory at Ilia State University (Iliauni, Georgia)

The 70 cm Meniscus telescope (focal length of 2460 mm) of the Abastumani Astrophysical Observatory (AbAO, 41°45′17″ N, 42°49′20″ E) was mounted in 1955 at the altitude of 1610 m. A pl4240-ccd-camera-back-illum-63-5mm-shutter-grade-1 with BVR_CI_C filters on the telescope provides an FoV of 30 arcmin × 30 arcmin, with a readout of 10 s. The limiting magnitude in the R_C filter with an exposure time of 1 min is 18.2 mag (AB system, $3-\sigma$). The 48 cm Cassegrain telescope (at an altitude of 1605 m) with an equivalent focal length of 7715 mm is equipped with an Apogee Alta KAF-16801E CCD together with $UBVR_CI_C$ filters, and has an FoV of 20 arcmin × 20 arcmin. The limiting magnitude in the R_C filter for an exposure of 1 min is 15 mag (AB system, $3-\sigma$).

2.3 HETH group at IAA

The HETH (**H**igh **E**nergy **T**ransients and their **H**osts) group, a research group at the Instituto de Astrofísica de Andalucía (IAA) in Granada, Spain, contributes with three different observing programmes to the GRANDMA consortium. All the telescopes' allotted time has been obtained in competitive calls for observing time for semesters 2019A and 2019B.

The Javalambre Auxiliary Survey Telescope (JAST/T80) is an 83 cm, F4.5 survey telescope located at the Javalambre observatory[4] in Teruel, Aragón, Spain, at an altitude of 1082 m at 40°02′33.7″ N and 1°00′59.6″ W. The telescope is equipped with the T80-cam installed at the Cassegrain focus, with an FoV of 1.4° × 1.4° and 12 SDSS and narrow-band filters. The camera has a 9.2k × 9.2 k CCD with 10 μm pixels, which yields a pixel scale of 0.55 arcsec pixel^{-1}. This telescope is used for tiling observations (proposals # 1800140,1800150,1900160, PI Kann) to cover parts or the full error box during the first night, taking up to 50 pointings of 180 s in the r' band with a limiting magnitude of 21 per tile. A second part of the programme allows for follow-up of a counterpart (e.g. a KN) in the i' band for up to ∼2 weeks, reaching a limiting magnitude of $i' > 22$ mag in a 600 s exposure.

The second facility is the Observatorio de Sierra Nevada[5] (OSN), managed by IAA and located at an altitude of 2896 m in the Sierra Nevada ski resort in Granada, Spain, at 37°03′46.4″ N and 3°23′09.8″ W. The 150 cm telescope at OSN is equipped with an Andor iKon-LDZ936N 2048 × 2048 pixel camera in the Nasmyth focus and has an FOV of 7.92 arcmin × 7.92 arcmin. This camera is used to detect possible counterparts in candidate hosts, for which we use the Johnson–Cousins R_C filter (2019/1 PI Izzo, 2019/2 PI Blazek). An additional run to follow up a possible KN in BVR_CI_C filters is also included, reaching $\sim I_C = 21$ mag in a 540 s exposure.

Finally, we use several instruments at the Centro Astronómico Hispano Andaluz (CAHA) observatory[6] at the Sierra de Los Filabres, Spain, at an altitude of 2196 m, at 37°13′23.4″ N and 2°32′45.6″ W, also managed by the IAA. We use the Bonn University Simultaneous Camera (BUSCA), mounted at the Cassegrain focus of the 2.2 m telescope, for follow-up of GW counterparts or KNe in different filters (2019F-15, 2019H-22, PI Kann). The Calar Alto Faint Object Spectrograph (CAFOS), also mounted on the 2.2 m telescope, is used for imaging and spectroscopic follow-up of sufficiently bright candidate counterparts (2019F-16, 2019H-23, PI Kann). CAFOS is an imager and spectrograph that we use with the B400 grism, which has a limiting magnitude of ∼21 mag in a 1h exposure.

[3]At each observatory location, the night time is chosen to start when the local Sun elevation is below −13°. The local sky visible area is defined with all the pointings having a local elevation of 25° above the local horizon, with no restriction on the western and eastern hour angle accessible by each telescope.

[4]https://oajweb.cefca.es
[5]https://www.osn.iaa.csic.es
[6]https://www.caha.es

2.4 Observatoire de Haute-Provence

IRiS (Initiation to Research in Astronomy for Schools) is a robotic telescope installed in 2013 on the site of the Observatoire de Haute-Provence, France, in order to allow for discoveries in the transient sky, while offering the opportunity to learn modern observational techniques. The telescope is a Ritchey–Chrétien-type telescope with a diameter of 50 cm mounted on a German-type mount and equipped with a focal plane composed of a camera equipped with an E2V 42–40 sensor (2k × 2k), a filter wheel, and filters (Clear, SDSS $u'g'r'i'z'$, as well as narrow bands centred on the Hα, CH_4, and OIII lines). The entire telescope and its equipment can be fully controlled remotely in order to automatically follow up interesting transients or perform a series of targeted exposures of known galaxies to find optical counterparts of GRBs, GWs, and neutrino events.

In the case of optical counterparts deemed significant, we can use the T120 telescope, also located at Observatoire de Haute-Provence. It is a 120-cm-diameter telescope equipped with an Andor Ikon L 936 camera with a 2048 × 2048 CCD with an FoV of 13.1 arcmin × 13.1 arcmin and with BVR_CI_C filters.

2.5 Les Makes observatory

The 60 cm telescope at Les Makes Observatory (Réunion Island) is a Ritchey–Chrétien F/8 reflector. A SBIG ST11K CCD camera with Astronomik LRGB filters provides an FoV of 26 arcmin × 17 arcmin. A typical exposure uses a 3 × 3 binning, providing a spatial sampling of 1.16arcsec pixel^{-1}. The telescope and camera are controlled by the AUDELA software using the RobObs script. This combination is adapted for galaxy targeting.

2.6 Lisnyky observatory

The 70 cm F/4 telescope at the observational station Lisnyky of Taras Shevchenko National University of Kyiv, Ukraine, is equipped with a FLI PL4710 back-illuminated CCD and *UBVRI* Bessel filters. For faint objects we use a mode with 2 × 2 binning, which gives a scale of 1.96 arcsec pixel^{-1}. The FoV of the instrument is 16 arcmin × 16 arcmin. The limiting magnitude of a 300 s exposure image is 20 mag under good sky conditions. It is possible to reach 21.5–22 mag with 1800 s exposures.

2.7 Shamakhy Astrophysical Observatory of Azerbaijan

The 60 cm telescope at Shamakhy Astrophysical Observatory (ShAO, 40°46′20″ N, 48°35′04″ E) (original equivalent focal length was 7.5 m) Schmidt–Cassegrain system was mounted in 1975 at an altitude of 1500 m. For use with GRANDMA collaboration observations, this telescope has been modified, with the equivalent focal length being reduced to 4.7 m. It is equipped with an FLI CCD camera with 4k × 4k pixels with size 9 μm and standard BVR_CI_C filters, which provides an 17 arcmin × 17 arcmin FoV with a readout time of 6 s. The limiting magnitude in the R_C filter of a 300 s exposure image is 19 mag with precision $3-\sigma$ under good sky conditions.

The 2 m telescope at Shamakhy Astrophysical Observatory (Coude, Cassegrain and direct focuses) was mounted in 1967 at an altitude of 1435 m. This telescope has been equipped with various spectrographs for spectral observations. For faint objects we can use a 2 × 2 Kanberra prism spectrograph. Typical observations in the visual range cover 3700–8000 Å up to 17 mag with a resolution of $R = 2000$.

2.8 TAROT network

TAROT stands for Télescope à Action Rapide pour les Objets Transitoires (Rapid Action Telescope for Transient Objects). Two TAROT 25-cm-aperture telescopes (Klotz et al. 2008) are installed at Calern in France (hereafter TCA) and La Silla in Chile (hereafter TCH). Initially designed to study optical counterparts of GRBs, these telescopes are now able to react to GW alerts. Their FoV is 1.86° × 1.86°. TAROT Réunion (hereafter TRE) is an 18-cm-aperture telescope that has been installed in 2016 at Les Makes observatory (Klotz & Thierry 2019). TAROT Réunion is located at 21.1988° S, 55.4102° E, and an elevation of 991 m above sea level. Its camera is an FLI 16803 that covers an FoV of 4.2° × 4.2° to be efficient when tiling the large skymaps delivered by GW interferometer alerts.

2.9 Tsinghua-NAOC Telescope

The Tsinghua-NAOC (National Astronomical Observatories of China) Telescope, abbreviated as TNT, is an 80 cm Cassegrain reflecting telescope located at Xinglong Observatory(117°34′39″ E, 40°23′40″ N, elevation: ∼900 m). It was designed and manufactured by APM-Teleskope in Germany and is under joint operation of Tsinghua University and NAOC since 2004. The main scientific goal of this telescope is to monitor and obtain photometric data of multiple transient phenomena such as supernovae, active galactic nuclei, and gamma-ray bursts .

This telescope is equipped with a 1340 × 1300 CCD camera providing an FoV of 11.5arcmin × 11.2 arcmin. The filter system used on the TNT is a standard Johnson *UBV* and Cousins R_CI_C system (Bessell 1990). The limiting magnitudes of TNT for an S/N of 100 with a 5 min exposure are 18.8 mag in the *V* band and 18.7 mag in the R_C band (Huang et al. 2012).

2.10 Zadko collaboration

The Zadko Telescope (Coward et al. 2010, 2017) is a 1 m Cassegrain telescope (with aperture *f*/4), located in Western Australia at coordinates 115°42′49″ E 31°21′24″ S. It has been designed by DFM Engineering Ltd and donated to the University of Western Australia by the resource company Claire Energy. The telescope has been active since the first of 2009 April, with various upgrades done when needed (see Coward et al. 2017, for details). For the O3 run, a new QHY 163M camera with a field of view of 17 arcmin × 12 arcmin has been installed, allowing for reaching $R \sim 21$ mag in about 90 s.

The telescope is controlled by the same software as the TAROT network, Robotic Observatory Software (ROS), aimed at observing the transient sky as quickly as possible when something occurs in the Universe. Like any ROS-compliant instrument, the Zadko Telescope is unsupervised, with various pipelines in charge of listening to several alert channels and to schedule, perform, process, and calibrate the observations. In the special case of GRANDMA, Zadko bypassed some of them as GRANDMA offers its own tools (see below).

In addition to the transient sky, the Zadko telescope is also used to perform outreach and teaching activities, and to study minor bodies in our Solar system. Lastly, the Zadko telescope also collaborates with other entities (such as NASA) to perform on-demand observations for full-time coverage, due to its unique location: This is the only 1-m-class professional telescope located

in Western Australia, which is located at the antipodes of the US mainland.

2.11 UBAI collaboration

The Ulugh Beg Astronomical Institute (UBAI) recently joined the GRANDMA project with two Zeiss-600 0.6 m Cassegrain telescopes (with an aperture *f*/12.5), Northern (NT-60) and Southern (ST-60). Both are located at the high-altitude Maidanak Observatory (66°54′ E, 38°40′ N, 2600 m above sea level; http://www.maidanak.uz) in the south-east of Uzbekistan at a distance of about 120 km south of Samarkand. The site provides about 60 per cent of the available yearly dark time (∼1800 h) with median seeing 0.69 arcsec at 0.5 μm (Ehgamberdiev et al. 2000). The maximum amount of Cear time corresponds to the summer–autumn period.

Operational since the 1980s, the telescopes are presently equipped with FLI 1024 × 1024 CCD cameras and *BVRI* Bessel filters, the FoV is 10.8 arcmin × 10.8 arcmin for the NT-60 and 6.5arcmin × 6.5 arcmin for the ST-60. The limiting magnitude in the *R* filter is 18 mag with a 3 min exposure.

2.12 Collaboration with other groups

GRANDMA can follow up counterpart candidates with two Chinese consortia that have synoptic surveys. First, the Tsinghua Mahuateng Telescopes (TMTS) are composed of 4 cm × 40 cm tubes on a single mount, located at Xinglong Observatory in Hebei Province, China. Each tube has a field of view of about 4.4 square degrees and resolution of 1.8 arcsec pixel^{-1}. It can reach 19 mag (5σ) in 60 s. Every night, the TMTS can scan about 8000 square degrees of the sky to search for optical transients such as supernovae and flare stars.

Secondly, GRANDMA also collaborates with Space-based multi-band astronomical Variable Objects Monitor (SVOM), a Sino-French Collaboration preparing a mission dedicated to the study of the multimessenger transient sky with a core programme devoted to GRB science (Wei et al. 2016). Currently, the SVOM ground segment used for O3 is mainly located in China at the Jilin and Xinglong Observatories. The full network has multiple photometric capabilities with:

(i) A 1.2 m Chinese Ground Follow-up Telescope (C-GFT at Jilin) equipped with a 4k × 4k CCD camera observing with no filter ($r_{\rm lim} \sim 20$ with 100 s exposure). The FoV of this telescope is 1.5° × 1.5° (1.35arcsec pixel^{-1} angular resolution).

(ii) Three Ground Wide-field Angle Cameras (GWAC at Xinglong) telescopes, each equipped with four 'JFOV' 4k × 4k CCD E2V camera ($\oslash = 18$ cm) and one 'FFOV' 3k × 3k CCD camera ($\oslash = 3.5$ cm). One mount has an FoV of 25° × 25° (∼500 deg^2) and typically a limiting unfiltered magnitude of 16 is reached with an exposure of 10 s (up to 18 at best by stacking hundreds of single images). The GWACs perform a systematic survey of the sky every night with online analysis of any discovered transients (Turpin et al. 2019a).

(iii) Two 60 cm telescopes (GWAC/F60A and GWAC/ F60B at Xinglong) equipped with 2k × 2k and 1k × 1k CCD cameras using $UBVR_CI_C$ Johnson–Cousins filters. With an FoV of ∼20 arcmin × 20 arcmin, they have a typical 1 arcsec angular resolution and a limiting magnitude of $R_{\rm lim} \sim 19$ mag in a 120 s exposure.

(iv) A 30 cm telescope (GWAC/F30 at Xinglong) is also operated with $UBVR_CI_C$ Johnson–Cousins filters with a quite wide FoV of 1.8° × 1.8° and $R_{\rm lim} \sim 17$ mag in a 100 s exposure.

Besides, in case of significant optical candidates during a GW alert, GRANDMA can trigger both photometric and spectroscopic observations on the two Chinese 2-m-class telescopes through the GRANDMA collaborators.

(i) The 2.16-m telescope, located at the Xinglong Observatory, has Cassegrain and Coude focuses, and it is simple to change from one to the other (only needing1 min). It is equipped with the BFOSC (Beijing-Faint Object Spectrograph and Camera), OMR Low Resolution Spectrograph, and HRS (High Resolution Fiber-Fed Spectrograph) as shown in Table 2.

(ii) The GMG 2.4-m telescope is located at the Lijiang station of Yunnan Observatories, and is similar to the Liverpool and Nordic Optical telescopes. It is equipped with the YFOSC (Yunnan Faint Object Spectrograph and Camera), and with a back-illuminated 2048 × 4096 E2V42-90 CCD. Using YFOSC, the limiting magnitude in photometry varies from 22 to 23 mag depending on the exposure time and the seeing. For low/medium spectral resolution observations, we expect a magnitude limit of about 19 mag depending on features in the spectrum.

GRANDMA obtained 10 h per semester of target-of-opportunity time for Semesters 2019 A and B on the Canada–France–Hawaii telescope (CFHT) equipped with WIRCAM and MegaCam, on the Big Island, Hawaii, United States, which can reach a 24 mag limit. We will use both of them for following up counterpart candidates of GW alerts in the optical and NIR band ($g'r'i'z'$ for MegaCam, *JH* for WIRCAM) and characterize the colour evolution of the kilonovae. In addition, MegaCam can participate in the GW skymap observations and to find directly the optical counterparts by targeting galaxies inside the GW volume.

GRANDMA is also connected to gamma-ray counterpart searches of GWs. First, we have developed our own offline detection pipeline to detect GRBs called F-WBSB (*Fermi*/GBM-like search with Wild Binary Segmentation for the detection of Bursts) presented in Antier et al. (2019a). In case of GW alerts, we extract archival data over the full day both in the *Fermi*/GBM and *INTEGRAL* SPI/ACS instruments. We consider a gamma-ray transient as interesting in the [−10 min, 1 hour] time window around the GW trigger. The pipeline gives an independent approach from standard online and offline analysis (Blackburn et al. 2015; Burns et al. 2019), which helps to confirm subthreshold triggers found by other groups with unique algorithms based on binary segmentation (Fryzlewicz 2014).

2.13 Citizen science programme

GRANDMA has also developed its own citizen science programme called *kilonova-catcher*[7]: Amateur astronomers having any observational capabilities are invited to participate in the follow-up of GW alerts. The participants are welcomed to register on the GRANDMA platform and to provide their telescope characteristics and location.

In case of a GW alert, induced by the merging of two compact objects involving at least one neutron star at a maximal distance of 200 Mpc, GRANDMA will compute a list of galaxies consistent with the distance range of the GW event as well as its sky localization given by the probability skymap (see Section 3.3). According to the telescope information given by each *kilonova-catcher* user, a short list of promising GW host galaxy candidates will then be automatically assigned to a telescope user using Slack

[7]https://grandma-kilonovacatcher.lal.in2p3.fr/

alert messages, emails and also displayed on the GRANDMA amateur platform on the telescope user page. The *kilonova-catcher* users are then encouraged on a best-effort basis to point their instruments towards those galaxies centred in their FoV and to adapt their exposure time to reach at least 17–18 mag. This limiting magnitude is based on the scenario of the kilonova AT 2017gfo detected in association with GW170817 (Abbott et al. 2017c). The images, in the FITS format, are then stored using an uploading application on the GRANDMA platform. If the electromagnetic counterpart is found during the global follow-up of any GW event, we will look back at the archival *kilonova-catcher* data to find if the field was observed by some amateur telescopes. If so, then the images will be reduced and the observations will be integrated into the full scientific analysis. Some amateur astronomers have acquired significant experience in searching for optical transient sources, particularly in the supernova domain. Their experience will be also profitable to potentially send promising optical transient candidates to a committee of GRANDMA scientists who will analyse them and take the decision to trigger deeper follow-up observations with the professional instruments.

Presently, GRANDMA reaches a participation of about 30 amateur astronomers across the world. 16 telescopes representing 60 per cent of the participants are located in France, the others mostly in Europe, especially in Spain with four telescopes. Other locations cover some regions in Canada, Chile, Mexico, Germany, Luxembourg, Malta, Mauritania, Australia, and New Zealand. The diversity of telescopes varies from 80 mm aperture to 600 mm with an average FoV of 40 arcsec. Their expected limiting magnitude for a 1 min exposure is about 17 mag with a resolution of 1.05 arcsec pixel^{-1}. A few of the telescopes are remotely operated, especially the largest ones, but most of the amateur astronomers directly control their telescope, sitting to the side of the pillar of their instruments. Nowadays, the amateur community has well-advanced skills in optical data-reduction techniques thanks to extensive tutorials given by many astronomical associations and specialized websites. Therefore, the non-professional world is perfectly able to produce data that are scientifically exploitable.The instantaneous coverage in different optical bands of the GW probability skymap by multiple telescopes will result in the unique opportunity to catch the early stage of the visible components of the post-merger ejected material.

3 OBSERVATION STRATEGY DURING THE LIGO/VIRGO O3 OBSERVATIONAL CAMPAIGN

3.1 Organization of the follow-up procedure

In order to perform follow-up of alerts and possible associated transients, a system of shifts has been set up, with a team of four follow-up advocates (FA) or 'shifters' designed to cover a entire week. Each day of a given week is divided in four 6-h-long shifts, each under the supervision of one FA. In principle, each FA is assigned the same daily slot during the week. In case of an alert, the first responsibility of the FA is to check that the observation plan has been computed, sent to the network of observatories, and has been well received by them. The FA has then to follow all notices (GCNs) related to the alerts currently in hand.

If an optical transient is found during the campaign (by GRANDMA or by others) and the first observations can be consistent with a kilonova or GRB afterglow signal, the FA may ask to follow it up by dedicated telescopes of the network. This may require the interruption of current observations for some telescopes and the modification of the observation plan. When a counterpart is formally identified (by the GRANDMA network or by others), the FA may also ask for observations by spectroscopic facilities of the network (the CAHA 2.2-m telescope, e.g.) or through ToO programmes we have access to.

Lastly, the FA is in charge of reporting everything that happened during their shift, either internally through a system of logbooks, or towards the whole community using an automatic writing tool generating the GCNs related to GRANDMA observations and possible discoveries.

3.2 GRANDMA infrastructure

Like any project aimed toward robotic astronomy and studying the transient sky, the GRANDMA project relies heavily on a central data base and cloud applications, developed for that purpose. We also constructed a dedicated web interface for helping the FA in their tasks.

At the core of the project lies a MySQL data base centralizing all information about the alerts and the observations done by any of the telescopes of the collaboration. That data base is populated automatically by various scripts, provided by the collaboration, and running at the telescope sites, or by programs running on our main server. It is accessed by some scripts that need specific information about the collaboration (i.e. our tool dedicated to produce GCNs sent by the collaboration) and the ongoing observations (the position of the tiles already observed, e.g.).

Each time a new event is detected by the aLIGO/Virgo collaboration and released to the public via a GCN, our server automatically retrieves and analyses the sky map of the error box of the event. It then produces a set of observation plans optimized for each telescope, following the method presented in the next section. That observation plan is then propagated to the observers. All of these mechanisms widely use the IVOA[8] methods for sharing data and information.

A web interface to the database allows at any moment to follow the ongoing procedure and adjust the observation strategies if needed. As a matter of consequence, each new detection of a GW counterpart candidate can be inserted into the database and followed up by small FoV instruments and/or spectroscopic instruments. That interface provides the only possible human supervision of the infrastructure, and is made for the benefit of the FAs.

3.3 Observation strategy for GW alerts

The beginning of O3 has provided a wide variety of GW candidates for follow-up, in terms of both the merging objects and the sky localization areas requiring examination. Due to the large sky localizations and differences in telescope configurations and sensitivities, optimized techniques for follow-up efforts are important. The GRANDMA observation strategy uses different approaches depending on the FoV of the telescopes. The core of the observation plans relies on `gwemopt` (Coughlin et al. 2018a), open-source software designed to optimize the scheduling of target-of-opportunity observations using either synoptic or galaxy-targeted searches. Briefly, for synoptic survey instruments ($\gtrsim$1 deg^2), it divides the skymap into a grid of 'tiles' the size and shape of the FoV of each telescope. For each tile the available segments for

[8] http://www.ivoa.net/

observation are computed, including accounting for their rising and setting, in addition to their distance from the moon. Observations are scheduled by computing a weight based on the three-dimensional probability distribution from the GW alert (Singer et al. 2016), for nearby sources ($\lesssim$300 Mpc), which are galaxy-weighted, following the distribution of galaxies and using their properties such as *B*-band luminosity. For narrow-FoV telescopes ($\lesssim$1 deg^2) with nearby alerts ($\lesssim$300 Mpc), galaxy-targeted observations are performed, where one galaxy at a time is imaged within the three-dimensional probability distribution, as suggested by Nissanke, Kasliwal & Georgieva (2013) and Gehrels et al. (2016).

Each observation is processed by the reduction pipelines to find transient candidates. In general, these images are compared to previous observations, either images or data bases of known objects (as traces of cosmics, known variable stars, minor planets, and known supernovae), to determine whether the objects are new with respect to the GW transient. For this reason, survey instruments with recent pre-existing limits are at an advantage in this endeavor. In addition, transients should have at least two detections separated in time to mitigate the follow-up of asteroids.

Each team of the GRANDMA consortium can use its own detection pipeline; a subset has low-latency reduction processes (the TAROT network, e.g.; Noysena et al. 2019). However, the GRANDMA consortium provides to individual teams a fast pipeline for the detection of potential new transients, called `gmadet`, which is publicly available through the GitHub platform.[9] The issue of new transient detection in the telescope images is complex and has several approaches. The error regions given by the aLIGO/Virgo interferometers are usually very large, significantly larger than any single observed image. An easy solution would be if every telescope in our network had previous images of the observed field from different periods. Those templates can be used for image subtraction, and new potential transients can be discovered afterwards by standard photometric techniques on the difference images. This approach is especially useful for the cases when the optical counterpart would be hidden visually inside the light of its host galaxy. However, telescopes in the GRANDMA network are not all-sky surveys and do not have a significant amount of templates for such an image subtraction. The situation is improved for those GW events with estimated distances inside the range of the GLADE catalogue of galaxies (Dálya et al. 2018). Those galaxies can be examined manually, and we can perform photometry for crowded fields (e.g. DAOPHOT) for the detection of optical candidates. However, most of the events are outside of the GLADE catalogue range. Therefore, the optical candidates can be practically anywhere in the telescope images.

In GRANDMA, there are various differences in the data reduction methods, including calibration and the filter systems employed. This can lead to differences in light curves that are not due to physical effects. Thus, the collaboration is working on a homogeneous procedure to calibrate the images such that they have photometric consistency. In order to harmonize the detection process among the telescopes, which is crucial to affirm source discoveries with independent observations, we developed a common algorithm written in the PYTHON programming language and using several external astronomical packages and modules to perform astrometry and photometry. The astrometric calibration is performed using the ASTROMETRY.NET package (Lang et al. 2010), the source detection is performed using either IRAF (Tody 1986) or SEXTRACTOR (Bertin & Arnouts 1996) depending on the user preference. After stellar detection we perform a cross-check of all detected sources with several astronomical catalogues, PanSTARRS, USNO-B1, Gaia, and GSC using the CDS X-match service. The final stage consists of photometry of the unidentified sources and then a subsequent upload of the potential transients into the GRANDMA internal database. Subimages centred on these potential transients are displayed on the web interface and compared to the same fields from the PanSTARRS all-sky survey using ALADIN LITE.[10] There is an ongoing effort to automatically discard artefacts among the transient candidates using a machine learning algorithm.

Follow-up of the remaining optical transients with dedicated telescopes is performed to classify them; this includes both photometric and spectroscopic follow-up. While classifying supernovae and M-dwarf flares spectroscopically is relatively straightforward, photometrically, one needs to rely on the rapid time-scales over which kilonovae evolve (Metzger 2017). Comparison to GW170817/AT 2017gfo shows that the evolution in luminosity is expected to be $\Delta r \sim 1$ mag d^{-1}, and slightly slower at later times; for this reason, transients can be ruled out by measurements of their luminosity evolution. In general, typical supernovae near peak evolve much more slowly ($\Delta r \sim 0.1$ mag d^{-1}) and therefore can be rejected by tracking their photometric evolution. In this way, the network can follow up objects both photometrically and spectroscopically to both classify and exclude sources. In parallel, the GRANDMA consortium is developing a similar approach to harmonize spectroscopic reduction with generic data pre-processing and calibration.

4 GRANDMA ELECTROMAGNETIC FOLLOW-UP CAMPAIGN OF O3 RUN A

4.1 Summary of the first six months of the campaign

The GRANDMA consortium followed up 27/33 alerts during the first six months of the O3 campaign, as shown in Table 3 for the BBH merger candidates and Table 4 for the systems containing at least one neutron star based on LIGO–Virgo low-latency results (see the LIGO–Virgo user guide for more information[11]). All the sky localizations of the alerts can be shown in Appendix A, (see Figures and Table A1).

We first note that none of our follow-ups have led to a complete coverage of any error box. This can be explained by the fact that Sun and Moon constraints do not allow us to perform full coverage (see the example of S190924h). In addition, the luminosity distances of the alerts sent by LIGO–Virgo are mostly above 150 Mpc (the closest BNS candidate was estimated to lie at 156 ± 41 Mpc), where the galaxy catalogue we are using to perform galactic tiling is no longer complete.

The TAROT telescopes fully automatically responded to any alert. This helped us to track down several issues in the data base and web interface, improving the entire GRANDMA system. From 2019 April to September, the delay between the GW trigger time and the first observation by the TAROT network decreased from several hours to dozens of minutes. While our first answer to an alert was delayed by more than 12 h, in 2019 September, the ICARE infrastructure was able to receive the GW alert and produce the observation plan and send it to all GRANDMA telescopes within 10–15 min. Then, the automatic TAROT pipeline

[9] http://github.com/dcorre/gmadet

[10] https://aladin.u-strasbg.fr/AladinLite/

[11] https://emfollow.docs.ligo.org/userguide/

Table 3. Summary of the GRANDMA observations during the first six months for BBH candidates. Observations are not necessarily continuous during the time interval. S190829u was retracted by the LIGO–Virgo collaboration due to a data quality issue. 90% c.r. corresponds to the 90% credible region of the latest sky localization area sent by LIGO–Virgo, δt to the delay with respect to the GW trigger, ΔT to the duration of the observations, Prob (%), Area (deg^2) to the coverage of GRANDMA compared to the latest revision of the sky localization area in percentage and in square degrees. From 2019 May 19 to 2019 June 2, TRE and TCH were under maintenance and there were bad observational conditions at the TCA site. S190924h was not observed due to moon constraints. The δt is dependant on the delay of the first sky localization area sent by the LVC.

Alert	Time (UTC)	Type	Dist (Mpc)	90% c.r. (deg^2)	Telescope	δt (h)	ΔT (h)	Lim. mag	Prob (%)	Area (deg^2)
S190930s	13:35:41	MG (95%)	709 ± 191	1748	GRANDMA	1.9	57.0	17–18	19.0	260
					TCA	4.4	55.2	18	5.1	68
					TCH	12.7	46.0	18	3.0	38
					TRE	1.9	31.4	17	18.0	242
S190924h	02:19:258	MG (99%)	548 ± 112	303			No observations			
S190915ak	23:57:02	BBH (99%)	1584 ± 381	318	GRANDMA	0.3	50.7	18	36.1	80
					TCA	0.3	50.7	18	36.1	80
S190828l	06:55:09	BBH (99%)	1528 ± 387	359	GRANDMA	1.2	49.7	17–18	12.6	294
					TCA	12.6	31.2	18	0.3	67
					TCH	1.2	49.7	18	11.5	69
					TRE	14.2	23.7	17	0.8	157
S190828j	06:34:05	BBH (99%)	1946 ± 388	228	GRANDMA	0.5	47.6	17–18	6.1	210
					TCA	12.5	31.3	18	2.7	67
					TCH	0.5	47.6	18	0.04	21
					TRE	15.6	23.4	17	3.4	122
S190728q	06:45:10	MG (52%)	874 ± 171	104	GRANDMA	0.5	50.2	17–18	88.3	180
					TCA	13.2	29.6	18	18.8	26
					TCH	0.5	50.2	18	23.2	56
					TRE	10.5	22.6	17	83.3	121
S190727h	06:03:33	BBH (92%)	2839 ± 655	151	GRANDMA	1.5	163.8	17–18	49.0	138
					TCH	1.6	163.8	18	48.4	68
					TRE	16.7	17.2	17	0.7	70
S190720a	00:08:36	BBH (99%)	869 ± 283	443	GRANDMA	0.3	30.8	17–18	11.0	161
					TCA	0.6	26.8	18	5.0	60
					TCH	1.7	29.4	18	4.0	50
					TRE	0.3	22.7	17	4.0	71
S190707q	09:33:26	BBH (99%)	781 ± 211	921	GRANDMA	5.7	14.1	17–18	14.6	128
					TCA	10.7	6.1	18	2.4	21
					TCH	13.4	6.3	18	4.0	25
					TRE	5.7	4.8	17	9.5	88
S190706ai	22:26:41	BBH (99%)	5263 ± 1402	826	GRANDMA	0.5	22.9	17–18	16.0	167
					TCA	0.6	22.7	18	0.27	22
					TCH	0.5	9.1	18	3.9	24
					TRE	3.2	2.0	17	11.8	121
S190701ah	20:33:06	BBH (93%)	1849 ± 446	49	GRANDMA	2.7	2.9	17	41.7	71
					TRE	2.7	2.9	17	41.7	71
S190630ag	18:52:05	BBH (94%)	926 ± 259	1483	GRANDMA	4.7	18.9	17–18	11.4	92
					TCA	4.7	3.0	18	8.9	21
					TRE	21.0	2.5	17	2.5	71
S190602aq	17:59:27	BBH (99%)	797 ± 238	1172			No observations			
S190521r	07:43:59	BBH (99%)	1136 ± 279	488			No observations			
S190521g	03:02:29	BBH (97%)	3931 ± 953	765			No observations			
S190519bj	15:35:44	BBH (96%)	3154 ± 791	967			No observations			
S190517h[a]	05:51:01	BBH (98%)	2950 ± 1038	939	GRANDMA	4.2	17.3	18	8.9	11
					TCH	4.2	17.3	18	8.9	11
S190513bm[a]	20:54:28	BBH (94%)	1987 ± 501	691	GRANDMA	0.7	12.9	18	23.5	45
					TCA	0.7	5.6	18	7.0	24
					TCH	6.0	7.5	18	16.7	21

Table 3 – *continued*

Alert	Time (UTC)	Type	Dist (Mpc)	90% c.r. (deg^2)	Telescope	δt (h)	ΔT (h)	Lim. mag	Prob (%)	Area (deg^2)
S190512at	18:07:14	BBH (99%)	1388 ± 322	252	GRANDMA	13.8	18.1	18	30.3	42
					TCA	25.5	5.8	18	7.2	22
					TCH	13.8	18.1	18	24	24
S190503bf[a]	18:54:04	BBH (96%)	421 ± 105	448	GRANDMA	4.3	4.7	18	17.1	24
					TCH	4.3	4.7	18	17.1	24
S190421ar	21:38:56	BBH (97%)	1628 ± 535	1444	GRANDMA	19.7	8.2	17	18.0	124
					TRE	19.7	8.2	17	18.0	124
S190412m[a]	05:30:44	BBH (100%)	812 ± 194	156	GRANDMA	10.1	12.2	17–18	75.9	125
					TCA	14.1	8.2	18	36.3	24
					TRE	10.1	7.7	17	73.4	123
S190408an[a]	18:18:02	BBH (100%)	1473 ± 358	387	No observations					

[a]When only 'the bayestar sky localization' is available.

(CADOR) (Bourez-Laas et al. 2008) was able to schedule the first observations to start within 5–15 min of one of the observatories. For some other telescopes, the insertion into the schedule needs human validation, which can take up to 1 h. We are working on reducing that time delay. The most rapid follow-up was for S190515ak, with a delay of 16 min between the GW trigger and the first observation of TAROT-Calern.

Lastly, the coverage of GRANDMA improved during the first six months from 100 to 300 deg^2 with a maximum coverage (for S190910d) of 540 deg^2 in 68 h thanks to a more efficient coordination of the telescopes.

We also highlight the participation of the OAJ/T80 to the S190426c alert, a BNS merger candidate; these observations covered 11 per cent of the sky localization probability at 19.6 mag in the r' band. We also triggered various telescopes with the S190425z alert discussed in Section 4.2. Finally, ShAO/T60, Lisnyky/AZT-8, and UBAI/NT-60 were triggered for the BNS candidate S190818y alert, using a galaxy-targeting strategy, for the purpose of demonstrating a generic photometric detection pipeline on all the observations. The follow-up activity increase also received help from a successful campaign with the amateur astronomers programme for the S190901ap BNS merger candidate alert, estimated at a luminosity distance of 241 ± 79 Mpc. For that event, we reached a coverage of 90 per cent of the credible region of 14 753 deg^2, pointing at some interesting galaxies contained in the GW volume (Ducoin et al. 2019).

Besides, our independent search for finding gamma-ray bursts in the *Fermi*-GBM data (Antier et al., in preparation) in the period of around the GW trigger time (−5 s, 1h) did not lead to any significant GRB detection.

Despite all our efforts, no significant counterparts were found by the GRANDMA consortium for any alert (in agreement with observations by other groups).

4.2 An example of follow-up: the binary neutron star merger candidate S190425z

4.2.1 S190425z: the first binary neutron star merger candidate of O3

The GW event S190425z occurred on 2019-04-25 at 08:18:05 UTC (LIGO Scientific Collaboration & Virgo Collaboration 2019). At that moment, both Advanced LIGO-Livingston and Virgo were observing, while Advanced LIGO-Hanford had been down for 30 min. The lack of a detection by LIGO-Hanford resulted in a very large localization region, with the initial 90 per cent credible region of the skymap for S190425z spanning ∼10 200 deg^2. A refined analysis reduced this region to ∼7500 deg^2.

The false-alarm rate of S190425z, an estimate of its significance, was ≈1 per 70 000 yr (see definitions in the the LIGO–Virgo user guide). The candidate also had a large probability to be a BNS merger and to have a remnant (both probabilities > 99 per cent). Finally, the distance, inferred from the GW signal, was estimated to be 156 ± 41 Mpc.

Due to these properties, an intense follow-up campaign occurred in the month following the event, with more than 100 notices sent by various teams via the GCN network.[12] Wide-field optical tiling collaborations like ZTF, ATLAS, Pan-STARRS, and Gaia discovered multiple optical counterpart candidates (Kasliwal et al. 2019b; Kostrzewa-Rutkowska et al. 2019a,b,c; McBrien et al. 2019; Smith et al. 2019a,b), but all turned out to be supernovae or other sources unrelated to S190425z (Buckley et al. 2019; Carini et al. 2019; Castro-Tirado et al. 2019; Chang et al. 2019; Dichiara et al. 2019; Dimitriadis et al. 2019; Izzo et al. 2019; Jencson et al. 2019; McCully et al. 2019; Morokuma et al. 2019; Nicholl et al. 2019b,c; Pavana et al. 2019; Perley, Copperwheat & Taggart 2019; Short et al. 2019; Wiersema et al. 2019). At high energies, no contemporaneous emission was detected by any satellites (Axelsson et al. 2019; Casentini et al. 2019; Chelovekov et al. 2019; Martin-Carillo et al. 2019; Minaev et al. 2019; Piano et al. 2019; Sakamoto et al. 2019; Savchenko et al. 2019; Sugizaki et al. 2019; Svinkin et al. 2019; Xiao et al. 2019). Neutrinos and cosmic rays were also not detected (Alvarez-Muniz et al. 2019; Icecube Collaboration 2019).

Several factors led to difficulties in finding the counterpart. First of all, the highly unconstrained localization led to ∼50 000 galaxies within the three-dimensional estimated volume (Cook et al. 2019; Dalya & Raffai 2019). It is challenging to observe even most of these galaxies several times in order to pinpoint a transient event. Secondly, the large distance (four times further than GW170817) implied that a kilonova similar to AT 2017gfo/GW170817 would appear two to three magnitudes fainter. Observing such a faint object implies an increase in exposure time required for each image (for a given telescope), leading to it being highly challenging to succeed in a detection during the first 12 h. Therefore, it

[12]https://gcn.gsfc.nasa.gov/other/GW190425z.gcn3

Table 4. Summary of the GRANDMA observations during the first six months for binary neutron star or neutron star–black hole merger candidates, using the latest versions of the LALInference sky localizations. Observations are not necessarily continuous during the time interval. S190518bb, S190524q S190808ae, S190816i, and S190822c were retracted by the LIGO–Virgo collaboration due to data quality issues in the detectors. 90% c.r. corresponds to the 90 % credible region of the latest sky localization area sent by LIGO–Virgo, δt to the delay with respect to the GW trigger, ΔT to the duration of the observations, Prob (%), Area (deg^2) to the coverage of GRANDMA compared to the latest revision of the sky localization area in percentage and in squares degrees. δt is dependant on the delay of the first sky localization area sent by the LIGO–Virgo collaboration; this generally took about a few hours at the beginning of the campaign.

Alert	Time (UTC)	Type	Dist (Mpc)	90% c.r. (deg^2)	Telescope	δt (h)	ΔT (h)	Lim. mag	Prob (%)	Area (deg^2)
S190930t[a]	14:34:07	NSBH (74%)	108 ± 38	24220	GRANDMA	1.0	80.5	17–18	1.3	250
					TCA	3.5	80.0	18	0.7	135
					TCH	11.9	71.5	18	0.6	110
					TRE	1.0	80.5	17	0.4	94
S190923y[a]	12:55:59	NSBH (68%)	438 ± 133	2107	GRANDMA	3.6	55.6	17–18	25.4	436
					TCA	5.5	46.3	18	2.2	64
					TCH	10.7	32.7	18	3.5	64
					TRE	3.6	55.6	17	20.0	312
S190910h	08:29:58	BNS (61%)	230 ± 88	24264	GRANDMA	10.5	129.1	18	1.1	337
					TCA	10.5	129.1	18	0.5	175
					TCH	25.0	113.1	18	0.6	161
S190910d	01:26:19	NSBH (98%)	632 ± 186	2482	GRANDMA	1.0	67.6	17–18	37	540
					TCA	1.0	67.6	18	4	103
					TCH	3.5	52.6	18	11	158
					TRE	18.3	44.2	17	32	360
S190901ap	23:31:01	BNS (86%)	241 ± 79	14753	GRANDMA	0.4	58.6	17–18	9.1	354
					TCA	1.25	57.4	18	2.5	100
					TCH	4.5	46.6	18	3.0	112
					TRE	0.4	48.6	17	7.2	279
S190814bv	21:10:39	NSBH (99%)	267 ± 52	23	GRANDMA	0.5	22.5	17–23	90.2	161
					TCA	0.65	13.5	18	21.9	32
					TRE	0.5	22.2	17	89.0	139
					LesMakes	1.3	3.6	18.5	6.1	2
					CFHT	232.0	0.5	23.0	<1	1
S190718y[a]	14:35:12	BNS (2%)	227 ± 165	7246	GRANDMA	3.9	54.6	17–19	48.8	120
					TRE	7.4	51.1	17	48.8	120
					Shao/T60	4.6	1.3	16.5	<1	<1
					UBAI/T60	3.9	1.5	18.0	<1	<1
					Lisnyky/AZT-8	5.7	2.8	19.2	<1	<1
S190510g	02:59:39	BNS (42%)	227 ± 92	1166	GRANDMA	2.1	69.3	18	45.0	51
					TCA	16.7	54.7	18	0.3	24
					TCH	2.1	68.3	18	44.7	31
S190426c	15:21:55	BNS (24%)	377 ± 100	1131	GRANDMA	6.3	60.5	17–20	28.6	152
					TCA	7.4	52.9	18	9.7	23
					TCH	15.4	51.4	18	4.3	25
					TRE	7.4	50.9	17	14.0	105
					OAJ	6.3	4.9	19.6	11.4	44
S190425z	08:18:05	BNS (99%)	156 ± 41	7461	GRANDMA	6.7	63.4	17–23	2.8	135
					TCA	38.1	29.1	18.0	0.9	18.0
					TCH	22.4	47.7	18.0	1.0	25
					TRE	6.7	33.6	17.0	2.4	124
					Zadko	6.7	28.0	16.0	<1	<1
						14.2	2.5	16.5	<1	<1
					Abastumani/T70					
					Lisnyky/AZT-8	14.8	2.2	19.2	<1	<1
					Les Makes/T60	7.0	8.5	19.2	<1	<1
					GMG/2.4	9.3	3.0	19.0	<1	<1
					CAHA/2.2	81.6	1.7	23.0	<1	<1

[a]When only 'the bayestar sky localization' is available.

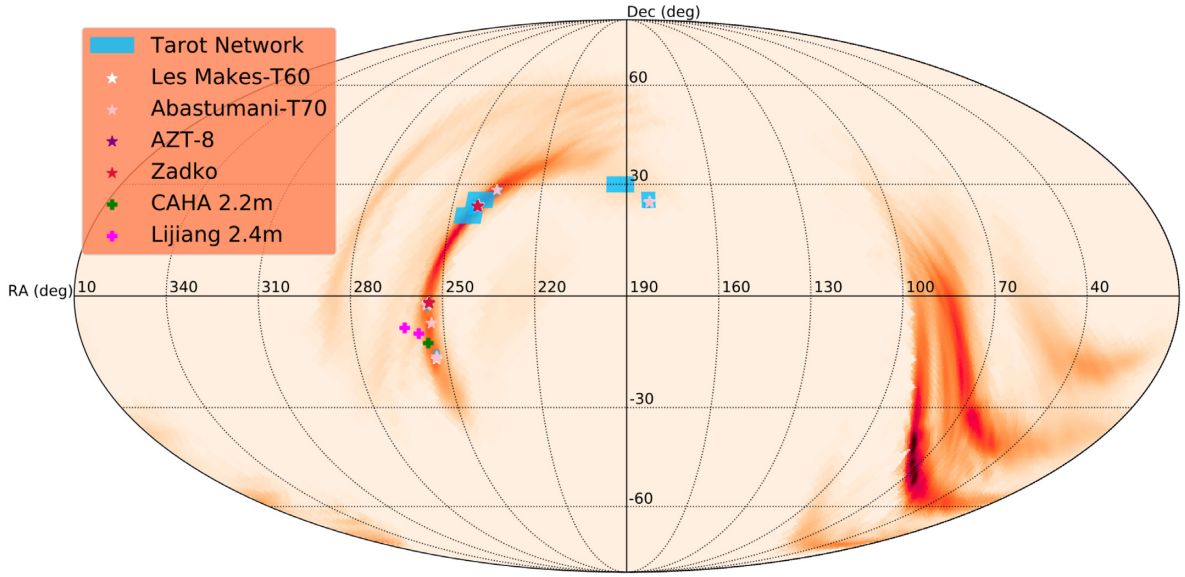

Figure 3. GRANDMA follow-up of the GW candidate event S190425z, a BNS merger candidate. Blue tiled areas represent observational tiles obtained by the TAROT network. In red, the LALInference sky localization area of S190425z is shown. Stars represent galaxy-targeted fields obtained by multiple observatories (see legend). Plus signs represent direct observations of candidate counterparts (not discovered by GRANDMA).

is not surprising that no significant candidate counterparts were discovered.

4.2.2 GRANDMA follow-up observations of S190425z

The LIGO Scientific Collaboration and the Virgo Collaboration sent a GCN notice 42 min after the trigger. Observation plans with both 'tiling' for the TAROT network and 'galaxy targeting' strategies for the other telescopes were computed automatically as described in Section 3. These plans were sent to the telescopes 15 min after the initial GCN reception.

A total of seven GRANDMA telescopes responded to this alert. The observations started in the following order: Zadko (2019-04-25 14:56:19 UTC, 6.7 h post GW trigger time), TAROT/TRE (2019-04-25 14:56:19 UTC, 6.7 h post GW trigger time), Les Makes/T60 (2019-04-25 15:18:10 UTC, 7.0 h post GW trigger time), Lisnyky/AZT-8 (2019-04-25 22:32:38 UTC, 14.2 h post GW trigger time), Abastumani/T70 (2019-04-25 23:08:01 UTC, 14.8 h post GW trigger time), TAROT/TCH (2019-04-26 06:40:5 UTC, 22.4 h post GW trigger time), and TAROT/TCA (2019-04-26 22:25:38 UTC, 1.6 d post GW trigger time).

The observations were previously reported in Blazek et al. (2019b), Howell et al. (2019b) and Gendre et al. (2019). The joint coverage of the alert is shown in Figs 3 and 4; the data are presented in Table 4. The TAROT network observed seven fields with multiple epochs per telescope corresponding to a few per cent of the initial Bayestar sky localization coverage (see Table B1 in the appendix). The Zadko telescope and camera were in test mode, with its sensitivity strongly decreased compared to its normal state; in total, images of 70 galaxies compatible with the GW distance were obtained in the five fields observed. The Les Makes/T60 recorded five images of 300 s each: 52 galaxies compatible with the GW distance were observed. Abastumani-T70 observed eleven fields containing 41 galaxies in the *R* band with a partly cloudy sky. Lisnyky/AZT-8 observed seven tiles with images of 26 potential host galaxies in the *R* and *B* bands. The full list of galaxies observed

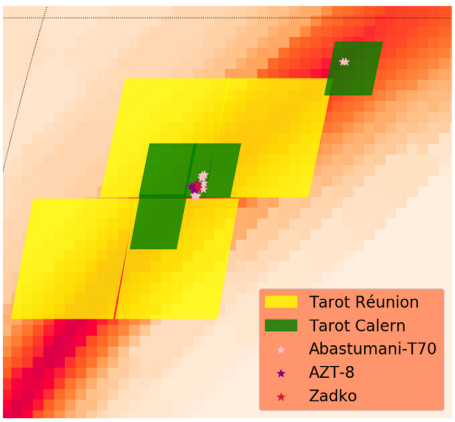

Figure 4. Zoom in to Fig. 3 to show details of the observation tiles and the galaxy-targeted follow-up. While the fields for each of the TAROT telescopes do not (or barely) overlap, a more efficient system of assigning tiles to prevent overlap across multiple telescopes (Coughlin et al. 2019c) had not been implemented here yet.

by Zadko, Les Makes/T60, Lisnyky/AZT-8, and Abastumani/T70 is available in Table B2 of Appendix B.

Each telescope team was in charge of the reduction of its own data, and each team used diverse techniques to search for new transients. The teams mostly compared their data with deeper archival imaging of the fields by hand, for example PanSTARRS, SDSS, or, if neither of those surveys covered this sky position, DSS. They also checked the Minor Planet Center data base[13] to see whether some spurious 'transient' was found to be a passing asteroid and therefore not related to the event. In addition, the TAROT network used a different method to find transients described in Noysena et al. (2019). There

[13] https://minorplanetcenter.net/cgi-bin/checkmp.cgi

were no reported counterpart candidates. The upper limit for the kilonova or orphan afterglow emission at 5σ in the sky localization area observed by GRANDMA was Clear $<$ 16 mag for Zadko, Clear $<$ 17 mag for the TAROT network, $R_C < 19.2$ for Les Makes/T60, R_C, $B < 19.2$ for Lisnyky/AZT-8, and $R_C < 16.5$ for Abastumani/T70.

The automatic observations of the event by the TAROT network favoured multi-epoch tiling observations in order to catch the rise of the potential kilonova emission. The localization was more than a factor of 100 larger than that of GW170817, which was used as our study case (Abbott et al. 2017a). Thus, the mapping of the skymap was far from optimal, with temporal redundancy not only in the same telescope but also in the full network. Also, the strategy employed for galaxies allowed overlap of fields. In this sense, S190425z helped to vet the full infrastructure and demonstrated our capacity to observe GW alerts with a high temporal cadence, albeit optimized for a smaller localization.

There are a variety of lessons learnt from this first BNS candidate. First of all, coordination of multicolour observations: the earliest observations of AT 2017gfo associated with GW170817 revealed that it was a very blue source (e.g. Evans et al. 2017), in contrast to the typical red colours of SNe, especially ones beyond peak. Secondly, we desire to better use the small-FoV instruments by preventing overlapping tiles by slightly shifting the fields imaged, in addition to incorporating automatic interruption for observing counterpart candidates. Finally, the time needed to process the images was underestimated, and the difference of pipelines between each group led to some uncertainties on the coherence of the data analysis. This motivates a universal data reduction.

4.2.3 External counterpart candidates found by ZTF and Swift *UVOT*

We also observed some of the candidate counterparts reported by other groups. We observed the candidates ZTF19aarykkb and ZTF19aarzaod reported by the Zwicky Transient Facility (Kasliwal et al. 2019b) with LJT. Multiple images were obtained in the g' and r' bands (Li et al. 2019), at two epochs for ZTF19aarykkb, as well as a single r' epoch of ZTF19aarzaod. Images from the PanSTARRS survey were used for template subtraction and stars from this catalogue for calibration. Both sources are clearly detected, and the derived magnitudes are comparable to those derived by other teams (Bhalerao et al. 2019; Burke et al. 2019; Castro-Tirado et al. 2019; Hiramatsu et al. 2019; Kilpatrick et al. 2019; Sun et al. 2019; Tan et al. 2019). However, both events were ruled out as a possible counterpart, as they were spectroscopically identified as Type II SNe (Buckley et al. 2019; Chang et al. 2019; Castro-Tirado et al. 2019; Dichiara et al. 2019; Izzo et al. 2019a; Nicholl et al. 2019a; Pavana et al. 2019; Perley et al. 2019; Wiersema et al. 2019).

More or less at the same time, *Swift* UVOT detected a bright, blue, fast-evolving optical transient (Breeveld et al. 2019). We triggered the 2.2 m CAHA telescope to obtain photometric and spectroscopic follow-up observations. However, before the observations had commenced, another group reported that the source had since strongly faded (Kong et al. 2019). For this reason, we cancelled the spectroscopic observations, requesting only photometric data, and detected the source in $R_C I_C$ but not in *UBV* (Kann et al. 2019a). It has been interpreted since as the UV-bright flare of a late dwarf star (Bloom et al. 2019; Lipunov et al. 2019b) and is therefore not related to S190425z.

4.3 Constraining kilonova properties

Following the presentation of the targeted follow-up observations by the GRANDMA network, we want to seek answers to these questions: Can we derive constraints on the observed GW transients from our GRANDMA observations, and which kind of EM transients would have been missed by our observations? For this purpose, we consider as an example Lisnyky/AZT-8's observation of the galaxy HyperLEDA 1109773, which was part of the S190425z follow-up campaign. HyperLEDA 1109773 is about 136.9 Mpc away and Lisnyky/AZT-8 reached a limiting magnitude of 19.2 mag in the R_C and B bands. From the missing transient observation, we know that only compact binary mergers in HyperLEDA 1109773 would be in agreement with our observations, for which the maximum R_C-band magnitude would be below 19.2 mag. For a quantitative interpretation of this statement, we follow Coughlin et al. (in preparation); i.e., we use the kilonova model of Kasen et al. (2017) in combination with a Gaussian process regression based interpolation (Doctor et al. 2017) to create a surrogate model for arbitrary light-curve and ejecta properties (see e.g. Coughlin et al. 2018b; Coughlin et al. 2019b) for details. Our analysis shows that only extremely high ejecta masses, $\sim 0.5\,M_\odot$ or larger, are slightly disfavoured by our observations; for comparison, the ejecta mass of GW170817 is estimated to be $\sim 0.05\,M_\odot$. Thus, from our observations alone, kilonovae associated with smaller ejecta masses might have been missed. Such considerations provide a natural limit for target identification for GW alerts with large distances. However, if aperture times are increased then the GRANDMA network can be successfully employed for target characterisation of already observed transients. This is of particular importance for the astronomical community, since typically a large number of potential transients are obtained from large sky surveys and, as discussed, the GRANDMA network provides a perfect tool to follow these up.

5 DISCUSSION: TOWARDS NETWORK OPTIMIZATION

There has been a significant effort to optimize single-telescope observations (see e.g. Gehrels et al. 2016; Ghosh et al. 2016; Rana et al. 2017; Coughlin et al. 2018a) for large target-of-opportunity sky areas in the context of time-domain astronomy. There are a variety of considerations when it comes to how to use a single system. For example, the difference in techniques between synoptic or galaxy-targeted searches is not always clear. While some telescopes have FoVs such that one or the other is clearly preferred, for systems with FoV ≈ 0.1 deg^2, the answer is less obvious. One may also consider the difference in sensitivities (and potentially filters) between systems, as well as the ability to react promptly to an alert and the time allocated to observe targets of opportunity. The use of a small-aperture system in the optical is likely to be significantly different from that of a large-aperture system in the near-infrared, even if both rely on galaxy targeting to search for counterparts.

A network-level optimization is much more complicated. For example, the differences in sensitivity and FoV potentially lead to significantly different search strategies within the same network. Moreover, there are often differences between the observatories on the policy regarding how to respond to different types of alerts, for example, binary neutron stars or binary black holes. A network that has both synoptic and galaxy-targeted systems may make choices as to whether covering overlapping parts of the sky is appropriate. The unequal distribution of the telescopes on Earth should also be

taken into account, with some regions having a higher concentration of telescopes and some regions only being covered by a single telescope. A centralized scheduler supervising all the telescopes will ideally be the best option, which can respond in real time to the availability of telescopes for the observations, accounting for GW sky localization regions and their updates with candidates. In reality, it is difficult to create such a scheduler due to a variety of reasons, including the political aspects of various programmes, target-of-opportunity approvals required every semester, detection-pipeline reactions to transients, and the diversity of independent schedulers.

The ideal answer to this likely depends on whether the systems have similar sensitivities to transients, as well as if it is possible to schedule coordinated observations between the systems. This includes accounting for the use of different filters or creating significant temporal separation between observations. These multi-epoch observations of the same transients can then be useful to provide a measurement of luminosity evolution or colour information on a given source. Beyond simply searching for new objects, there are also considerations of how they can be usefully followed up. Synoptic systems such as ZTF and MASTER as well as the space satellite *Swift* have been reporting dozens of new transients, e.g. for S190425z (Breveld et al. 2019; Coughlin et al. 2019a; Kasliwal et al. 2019b; Lipunov et al. 2019a), and in general, each object requires either photometric or spectroscopic follow-up to classify it.

In addition to the dedicated follow-up systems, perhaps large-aperture systems dedicated to deep photometry and spectroscopic classification (or both), many of the smaller aperture systems that begin the search for new candidates may be more useful for following up objects found either within or outside of the network.

6 CONCLUSION

The GRANDMA consortium presented in this paper, which is a global network of 21 telescopes with both photometric and spectroscopic facilities, located in 15 different observatories, aims to face the challenges of time-domain astronomy; in particular, it is set up for the case of large uncertainties in the localization of the transient phenomena as presented in Coughlin et al. (2019c). The network morphology has 24-h coverage and large availability of the telescopes, which helps to rapidly scan the GW sky localization area to ∼18th mag. The tools that have been set up for monitoring the full network include the joint agreement between the teams, the web interface, the uniform distribution of the observation plan, and the 24-h follow-up advocates on duty to revise observation plans in case of interesting candidates and updated sky localization areas.

Since the beginning of the third observational campaign organized by aLIGO/Virgo, O3, the GRANDMA programme has demonstrated its capacity to perform follow-up by observing 27/33 GW events. This includes scheduling the observations for rapidly scanning the GW localization area with the help of the amateur astronomer community (as for S190901ap), low-latency detection pipelines for detecting transients, and vetting and characterizing potential counterpart candidates.

One area of improvement going forward is to understand the optimal coordination of a network of this size. Coughlin et al. (2019c) present basic strategies for telescope networks, including ways to tile localizations with telescopes of different FoVs and depths. Still to be understood is, e.g., how an individual telescope might prioritize observations within its assigned fields, especially those overlapping with other systems. In addition, it will be important to understand how to incorporate the fact that certain systems may not be available for a particular follow-up campaign, such as due to limited target-of-opportunity time or engineering or other downtime. There is ongoing development to create updated dynamical observation plans. In addition to joint observations, GRANDMA is also focusing on the development of generic data analysis (to be deployed by 2020 January) and on the central multimessenger plateform ICARE to improve the full process as well as integrating new telescopes into its programme.

ACKNOWLEDGEMENTS

Parts of this research were conducted by the Australian Research Council Centre of Excellence for Gravitational Wave Discovery (OzGrav), through project number CE170100004. EJH acknowledges support from a Australian Research Council DECRA Fellowship (DE170100891). AdUP and CCT acknowledge support from Ramón y Cajal fellowships RyC-2012-09975 and RyC-2012-09984 and the Spanish Ministry of Economy and Competitiveness through project AYA2017-89384-P. DAK acknowledges support from the Spanish research project AYA2017-89384-P. MB acknowledges funding as 'personal tecnico de apoyo' under fellowship number PTA2016-13192-I. MC is supported by the David and Ellen Lee Postdoctoral Fellowship at the California Institute of Technology. SA is supported by the CNES Postdoctoral Fellowship at Laboratoire AstroParticule et Cosmologie. SA, AC, CL, and RM acknowledge the financial support of the UnivEarthS Labex program at Sorbonne Paris Cité (ANR-10-LABX-0023 and ANR-11-IDEX-0005-02). SA and NL acknowledge the financial support of the Programme National Hautes Energies (PNHE). DT acknowledges the financial support of the Chinese Academy of Sciences (CAS) PIFI post-doctoral fellowship program (program C). UBAI acknowledges support from the Ministry of Innovative Development through projects FA-Atech-2018-392 and VA-FA-F-2-010. IRiS has been carried out thanks to the support of the OCEVU Labex (ANR-11-LABX-0060) and the A*MIDEX project (ANR-11-IDEX-0001-02) funded by the 'Investissements d'Avenir' French government program. IRiS and T120 thank all the Observatoire de Haute-Provence staff for the permanent support. SB, NK, RN, and MV acknowledge the Shota Rustaveli National Science Foundation (SRNSF grant No 218070). TAROT has been built with the support of the Institut National des Sciences de l'Univers, CNRS,France. TAROT is funded by the CNES and thanks the help of the technical staff of the Observatoire de Haute Provence, OSU-Pytheas.

REFERENCES

Aasi J. et al., 2015, Class. Quantum Gravity, 32, 074001
Abbott B. P. et al., 2017a, Phys. Rev. Lett., 119, 161101
Abbott B. P. et al., 2017b, Nature, 551, 85
Abbott B. P. et al., 2017c, ApJ, 848, L12
Abbott B. P. et al., 2017d, ApJ, 848, L13
Acernese F. et al., 2015, Class. Quantum Gravity, 32, 024001
Alvarez-Muniz J., Pedreira F., Zas E., Kampert K. H., Schimp M., 2019, GRB Coordinates Network, 24240, 1
Andreoni I., Ackley K., Cooke J. et al., 2017, PASA, 34, e069
Antier S., Barynova K., Fryzlewicz P., Lachaud C., Marchal-Duval G., 2019a, preprint (arXiv:1909.10002)
Antier S. et al., 2019b, GRB Coordinates Network, 25593
Antier S. et al., 2019c, GRB Coordinates Network, 25594
Arcavi I., 2018, ApJ, 855, L23
Axelsson M., Bissaldi E., Kocevski D., Longo F., Omodei N., 2019, GRB Coordinates Network, 24266, 1

Baker T., Bellini E., Ferreira P. G., Lagos M., Noller J., Sawicki I., 2017, Phys. Rev. Lett., 119, 251301
Barynova K. et al., 2019a, GRB Coordinates Network, 25666
Barynova K. et al., 2019b, GRB Coordinates Network, 25780
Bauswein A., Baumgarte T. W., Janka H.-T., 2013, Phys. Rev. Lett., 111, 131101
Bertin E., Arnouts S., 1996, A&AS, 117, 393
Bessell M. S., 1990, PASP, 102, 1181
Bhalerao V., Kumar H., Karambelkar V., Waratkar G., Sharma Y., Anupama G. C., 2019, GRB Coordinates Network, 24201, 1
Bhattacharya M., Kumar P., Smoot G., 2019, MNRAS, 486, 5289
Blackburn L., Briggs M. S., Camp J., Christensen N., Connaughton V., Jenke P., Remillard R. A., Veitch J., 2015, ApJS, 217, 8
Blazek M. et al., 2019a, GRB Coordinates Network, 24162
Blazek M. et al., 2019b, GRB Coordinates Network, 24227, 1
Blazek M. et al., 2019c, GRB Coordinates Network, 24327
Bloom J. S., Zucker C., Schlafly E., Finkbeiner D., Martinez-Palomera J., Goldstein D. A., Andreoni I., 2019, GRB Coordinates Network, 24337, 1
Boer M. et al., 2019, GRB Coordinates Network, 24126.
Bourez-Laas M., Vachier F., Klotz A., Damerdji Y., Boër M., 2008, in Astronomical Telescopes + Instrumentation, SPIE, p. 9
Breeveld A. et al., 2019, GRB Coordinates Network, 24296, 1
Buckley D. A. H., Jha S. W., Cooke J., Mogotsi M., 2019, GRB Coordinates Network, 24205, 1
Burke J., Hiramatsu D., Arcavi I., Howell D. A., McCully C., Pellegrino C., 2019, GRB Coordinates Network, 24206, 1
Burns E. et al., 2019, ApJ, 871, 90
Capano C. D. et al., 2019, AAS, 51, 403.03
Carini R. et al., 2019, GRB Coordinates Network, 24252, 1
Casentini C. et al., 2019, GRB Coordinates Network, 24180, 1
Castro-Tirado A. J. et al., 2019, GRB Coordinates Network, 24214, 1
Chang S. W. et al., 2019, GRB Coordinates Network, 24260, 1
Chelovekov I., Pozanenko A., Minaev P., Grebenev S., 2019, GRB Coordinates Network, 24181, 1
Cook D. O. et al., 2019, GRB Coordinates Network, 24232, 1
Corre D. et al., 2019, GRB Coordinates Network, 25599, 1
Coughlin M. W. et al., 2018a, MNRAS, 478, 692
Coughlin M. W. et al., 2018b, MNRAS, 480, 3871
Coughlin M. W. et al., 2019a, preprint (arXiv:1907.12645)
Coughlin M. W., Dietrich T., Margalit B., Metzger B. D., 2019b, MNRAS, 489, L91
Coughlin M. W. et al., 2019c, MNRAS, 489, 5775
Coward D. M. et al., 2010, PASA, 27, 331
Coward D. M. et al., 2017, PASA, 34, e005
Creminelli P., Vernizzi F., 2017, Phys. Rev. Lett., 119, 251302
Crisp H. et al., 2019a, GRB Coordinates Network, 24549
Crisp H. et al., 2019b, GRB Coordinates Network, 25749
Dalya G., Raffai P., 2019, GRB Coordinates Network, 24171, 1
Dálya G. et al., 2018, MNRAS, 479, 2374
Dichiara S., Gatkine P., Durbak J., Troja E., Cenko S. B., Kutyrev A., Veilleux S., 2019, GRB Coordinates Network, 24220, 1
Dimitriadis G. et al., 2019, GRB Coordinates Network, 24358, 1
Doctor Z., Farr B., Holz D. E., Pürrer M., 2017, Phys. Rev., D96, 123011
Ducoin J.-G. et al., 2019, GRB Coordinates Network, 25688
Ehgamberdiev S. A., Baijumanov A. K., Ilyasov S. P., Sarazin M., Tillayev Y. A., Tokovinin A. A., Ziad A., 2000, A&AS, 145, 293
Eichler D., Livio M., Piran T., Schramm D. N., 1989, Nature, 340, 126
Evans P. A. et al., 2017, Science, 358, 1565
Ezquiaga J. M., Zumalacarregui M., 2017, Phys. Rev. Lett., 119, 251304
Fong W. et al., 2019, ApJ, 883, L1
Fryzlewicz P., 2014, Ann. Statist., 42, 2243
Gehrels N., Cannizzo J. K., Kanner J., Kasliwal M. M., Nissanke S., Singer L. P., 2016, ApJ, 820, 136
Gendre B. et al., 2019, GRB Coordinates Network, 24763, 1
Ghirlanda G. et al., 2019, Science, 363, 968
Ghosh S., Bloemen S., Nelemans G., Groot P. J., Price L. R., 2016, A&A, 592, A82
Goldstein A. et al., 2017, ApJ, 848, L14
Hallinan G. et al., 2017, Science, 358, 1579
Hiramatsu D., Arcavi I., Burke J., Howell D. A., McCully C., Pellegrino C., 2019, GRB Coordinates Network, 24194, 1
Hotokezaka K., Nakar E., Gottlieb O., Nissanke S., Masuda K., Hallinan G., Mooley K. P., Deller A., 2019, Nature-Astronomy, 3, 940
Howell E. J., Ackley K., Rowlinson A., Coward D., 2019a, MNRAS, 485, 1435
Howell E. et al., 2019b, GRB Coordinates Network, 24256, 1
Huang F., Li J.-Z., Wang X.-F., Shang R.-C., Zhang T.-M., Hu J.-Y., Qiu Y.-L., Jiang X.-J., 2012, Res. Astron. Astrophys., 12, 1585
Icecube Collaboration, 2019, GRB Coordinates Network, 24176, 1
Izzo L. et al., 2019, GRB Coordinates Network, 24208, 1
Jencson J., de K., Anand S., Kasliwal M. M., Andreoni I., Ahumada T., Perley D. A., 2019, GRB Coordinates Network, 24233, 1
Just O., Bauswein A., Pulpillo R. A., Goriely S., Janka H.-T., 2015, MNRAS, 448, 541
Kann D. A. et al., 2019a, GRB Coordinates Network, 24459, 1
Kann D. A. et al., 2019b, GRB Coordinates Network, 25781, 1
Kasen D., Metzger B., Barnes J., Quataert E., Ramirez-Ruiz E., 2017, Nature, 551, 80
Kasliwal M. M. et al., 2017, Science, 358, 1559
Kasliwal M. M. et al., 2019a, MNRAS
Kasliwal M. M. et al., 2019b, GRB Coordinates Network, 24191, 1
Kilpatrick C. D. et al., 2019, GRB Coordinates Network, 24212, 1
Klotz A., Thierry P., 2019, Experimental Astronomy. p. 41
Klotz A., Boër M., Eysseric J., Damerdji Y., Laas-Bourez M., Pollas C., Vachier F., 2008, PASP, 120, 1298
Klotz A. et al., 2019, GRB Coordinates Network, 25338, 1
Kong A., Tan H. J., Yu P. C., Ngeow C. C., Ip W. H., 2019, GRB Coordinates Network, 24301, 1
Kostrzewa-Rutkowska Z. et al., 2019a, GRB Coordinates Network, 24345, 1
Kostrzewa-Rutkowska Z. et al., 2019b, GRB Coordinates Network, 24354, 1
Kostrzewa-Rutkowska Z. et al., 2019c, GRB Coordinates Network, 24366, 1
Lang D., Hogg D. W., Mierle K., Blanton M., Roweis S., 2010, AJ, 139, 1782
Leroy N. et al., 2019, GRB Coordinates Network, 24631
LIGO Scientific Collaboration, Virgo Collaboration, 2019, GRB Coordinates Network, 24168, 1
Lipunov V. et al., 2019a, GRB Coordinates Network, 24167, 1
Lipunov V. et al., 2019b, GRB Coordinates Network, 24326, 1
Li W. X. et al., 2019, GRB Coordinates Network, 24267, 1
Lyman J. D. et al., 2018, NatAs, 2, 751
Margutti R. et al., 2018, ApJ, 856, L18
Martin-Carillo A., Savchenko V., Ferrigno C., Rodi J., Coleiro A., Mereghetti S., 2019, GRB Coordinates Network, 24169, 1
McBrien O. et al., 2019, GRB Coordinates Network, 24197, 1
McCully C. et al., 2019, GRB Coordinates Network, 24295, 1
Metzger B. D., 2017, Living Rev. Rel., 20, 3
Metzger B. D., 2019, Annals of Physics, 410
Metzger B. D., Bauswein A., Goriely S., Kasen D., 2015, MNRAS, 446, 1115
Minaev P., Pozanenko A., Grebenev S., Chelovekov I., 2019, GRB Coordinates Network, 24170, 1
Mooley K. P. et al., 2018, Nature, 561, 355
Morokuma T. et al., 2019, GRB Coordinates Network, 24230, 1
Nicholl M. et al., 2019a, GRB Coordinates Network, 24211, 1
Nicholl M. et al., 2019b, GRB Coordinates Network, 24217, 1
Nicholl M. et al., 2019c, GRB Coordinates Network, 24321, 1
Nissanke S., Kasliwal M., Georgieva A., 2013, ApJ, 767, 124
Noysena K., Klotz A., Boer M., Laugier R., Komonjinda S., Turpin D., 2019, ApJ, 886, 73
Pannarale F., Ohme F., 2014, ApJ, 791, L7
Pavana M., Anupama G. C., Kiran B. S., Bhalerao V., 2019, GRB Coordinates Network, 24200, 1

Perley D. A., Copperwheat C. M., Taggart K. L., 2019, GRB Coordinates Network, 24204, 1
Piano G. et al., 2019, GRB Coordinates Network, 24186, 1
Radice D., Dai L., 2019, Eur. Phys. J., A55, 50
Radice D., Perego A., Zappa F., Bernuzzi S., 2018, ApJ, 852, L29
Rana J., Singhal A., Gadre B., Bhalerao V., Bose S., 2017, ApJ, 838, 108
Resmi L. et al., 2018, ApJ, 867, 57
Ruan J. J., Nynka M., Haggard D., Kalogera V., Evans P., 2018, ApJ, 853, L4
Sakamoto T. et al., 2019, GRB Coordinates Network, 24184, 1
Savchenko V. et al., 2017, ApJ, 848, L15
Savchenko V., Ferrigno C., Martin-Carillo A., Rodi J., Coleiro A., Mereghetti S., 2019, GRB Coordinates Network, 24178, 1
Short P. et al., 2019, GRB Coordinates Network, 24215, 1
Singer L. P. et al., 2016, Astrophys. J., 829, L15
Smith K. W. et al., 2019a, GRB Coordinates Network, 24210, 1
Smith K. W. et al., 2019b, GRB Coordinates Network, 24262, 1
Stachie C. et al., 2019, GRB Coordinates Network, 24431
Sugizaki M. et al., 2019, GRB Coordinates Network, 24177, 1
Sun T. et al., 2019, GRB Coordinates Network, 24234, 1
Svinkin D. et al., 2019, GRB Coordinates Network, 24417, 1
Tan H. J., Yu P. C., Ngeow C. C., Ip W. H., 2019, GRB Coordinates Network, 24193, 1
The LIGO Scientific Collaboration, the Virgo Collaboration, 2019, ApJ, 886, 73
Tody D., 1986, in Crawford D. L., ed., Proc. SPIE Conf. Ser. Vol. 627, Society of Photo-Optical Instrumentation Engineers Conference series. SPIE, Bellingham, p. 733
Troja E. et al., 2017, Nature, 551, 71
Troja E. et al., 2018a, MNRAS, 478, L18
Troja E. et al., 2018b, MNRAS, 489, 1919
Turpin D. et al., 2019a, preprint (arXiv:1902.08476)
Turpin D. et al., 2019b, GRB Coordinates Network, 25847, 1
Wei J. et al., 2016, preprint (arXiv:1610.06892)
Wiersema K., Levan A. J., Fraser M., Steeghs D. T. H., Jonker P., Malesani D. B., Tanvir N. R., 2019, GRB Coordinates Network, 24209, 1
Xiao S. et al., 2019, GRB Coordinates Network, 24213, 1

APPENDIX A: SKY COVERAGE LINKS

Table A1. Sky coverage observations of the GRANDMA consortium during the first six months.

GW trigger	GRANDMA sky localization coverage Link	GCN report
S190930t	https://grandma-owncloud.lal.in2p3.fr/index.php/s/qEuqLP4MFC9aAst	–
S190930s	https://grandma-owncloud.lal.in2p3.fr/index.php/s/L9giV01FNOqOe7P	–
S190923y	https://grandma-owncloud.lal.in2p3.fr/index.php/s/u1xnw9MGczJm3R8	Turpin et al. (2019b)
S190915ak	https://grandma-owncloud.lal.in2p3.fr/index.php/s/55vKDfmLJzbHyBn	Kann et al. (2019b)
S190910h	https://grandma-owncloud.lal.in2p3.fr/index.php/s/fJdB1OS0Fj3Pg3t	Barynova et al. (2019b)
S190910d	https://grandma-owncloud.lal.in2p3.fr/index.php/s/yhviEDd1e633wJH	Crisp et al. (2019b)
S190901ap	https://grandma-owncloud.lal.in2p3.fr/index.php/s/F2xWVjaJdniTkWk	Barynova et al. (2019a), Ducoin et al. (2019)
S190828l	https://grandma-owncloud.lal.in2p3.fr/index.php/s/NmDYNp1AGY5BynT	Antier et al. (2019b)
S190828j	https://grandma-owncloud.lal.in2p3.fr/index.php/s/tG92ASJWw5C1tWV	Antier et al. (2019c)
S190814bv	https://grandma-owncloud.lal.in2p3.fr/index.php/s/IKRVU8DGxKtoIPK	Klotz et al. (2019), Corre et al. (2019)
S190728q	https://grandma-owncloud.lal.in2p3.fr/index.php/s/g55dL4wKghD3V5k	–
S190727h	https://grandma-owncloud.lal.in2p3.fr/index.php/s/ai1VdEgtcW48tbZ	–
S190720a	https://grandma-owncloud.lal.in2p3.fr/index.php/s/VTOjRQxVDU7Ze1g	–
S190718y	https://grandma-owncloud.lal.in2p3.fr/index.php/s/MHpMFRhy4TGVahI	–
S190707q	https://grandma-owncloud.lal.in2p3.fr/index.php/s/FeZLc99kDMZaMbM	–
S190706ai	https://grandma-owncloud.lal.in2p3.fr/index.php/s/5yS9dQQ26FQ8FKz	–
S190701ah	https://grandma-owncloud.lal.in2p3.fr/index.php/s/ImQadVEpsVit1h6	–
S190630ag	https://grandma-owncloud.lal.in2p3.fr/index.php/s/pfuQHsUBbJaFtSP	–
S190517h	https://grandma-owncloud.lal.in2p3.fr/index.php/s/j8EDTsfDQUDq1D4	Leroy et al. (2019)
S190513bm	https://grandma-owncloud.lal.in2p3.fr/index.php/s/tCCiIMIiYpnNYEX	Crisp et al. (2019a)
S190512at	https://grandma-owncloud.lal.in2p3.fr/index.php/s/BSbYZ2O5ZnHwna8	–
S190510g	https://grandma-owncloud.lal.in2p3.fr/index.php/s/ipgBWxLiyL1nDfJ	–
S190503bf	https://grandma-owncloud.lal.in2p3.fr/index.php/s/6MdspJUbp0n8uaq	Stachie et al. (2019)
S190426c	https://grandma-owncloud.lal.in2p3.fr/index.php/s/FeFP4EWVgi2ZE3p	Blazek et al. (2019c)
S190425z	https://grandma-owncloud.lal.in2p3.fr/index.php/s/tZTxGSoCEMc4fwG	Gendre et al. (2019), Kann et al. (2019a) Howell et al. (2019b), Blazek et al. (2019b)
S190421ar	https://grandma-owncloud.lal.in2p3.fr/index.php/s/08hcngYuxwONGWf	Blazek et al. (2019a)
S190412m	https://grandma-owncloud.lal.in2p3.fr/index.php/s/gyf5HfDVD7GS5GD	Boer et al. (2019)

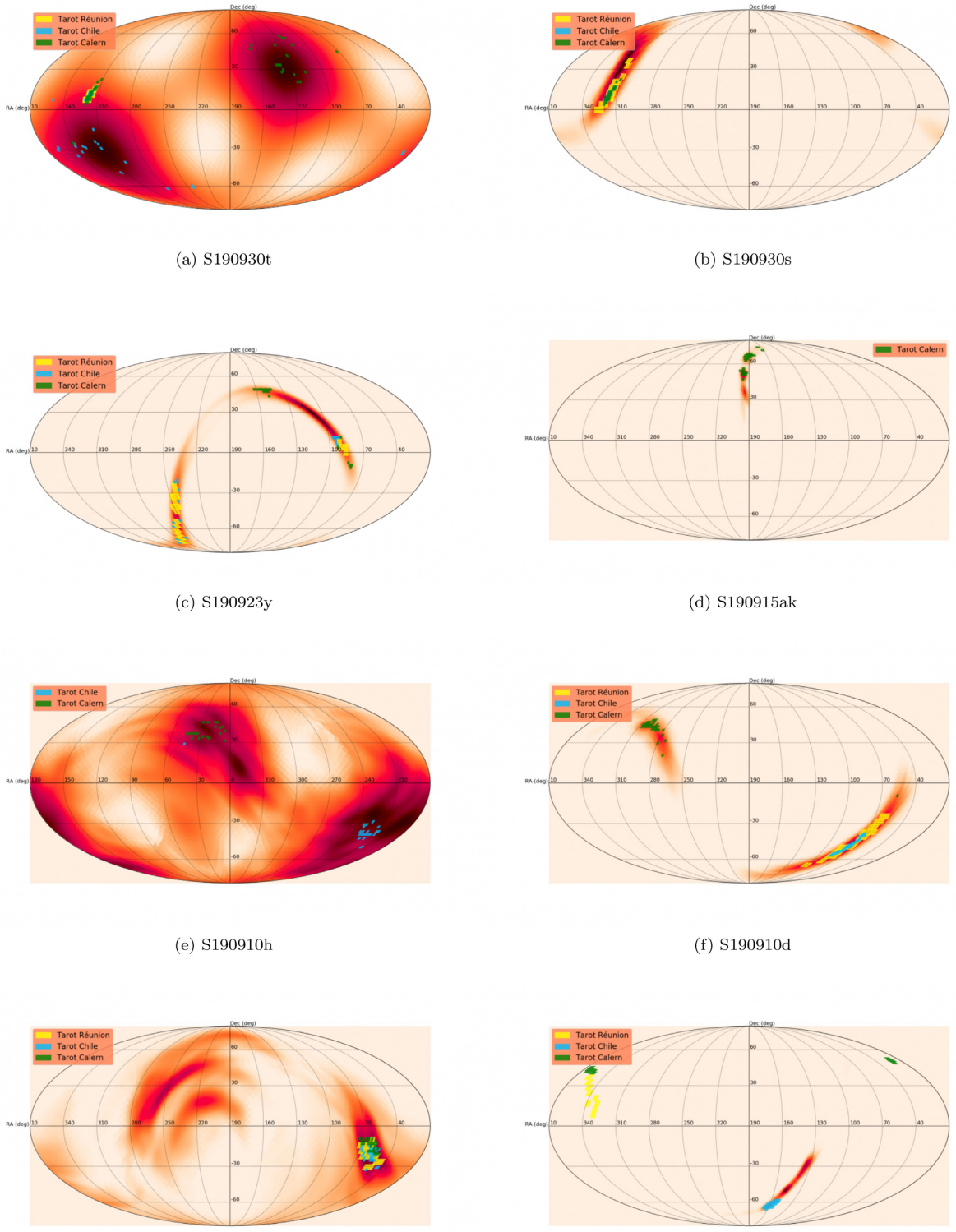

(a) S190930t

(b) S190930s

(c) S190923y

(d) S190915ak

(e) S190910h

(f) S190910d

(g) S190901ap

(h) S190828l

Figure A1. Sky coverage observations of the GRANDMA consortium during the first six months.

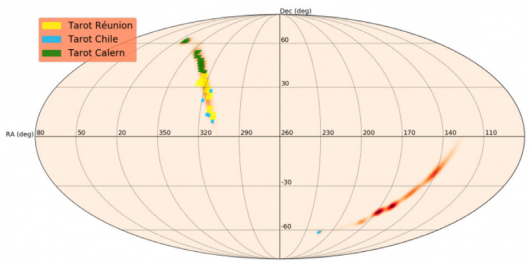

(a) S190828j

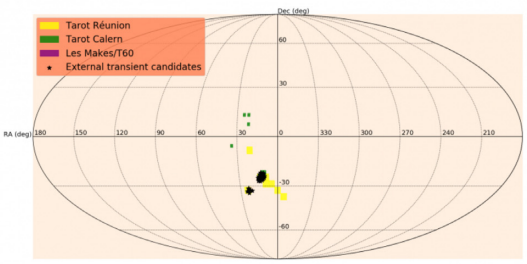

(b) S190814bv

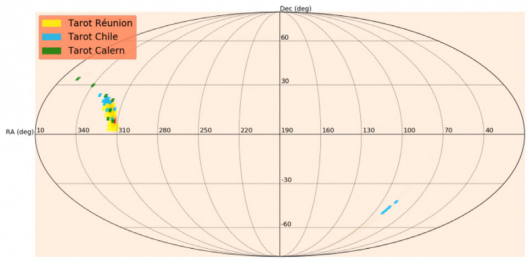

(c) S190728q

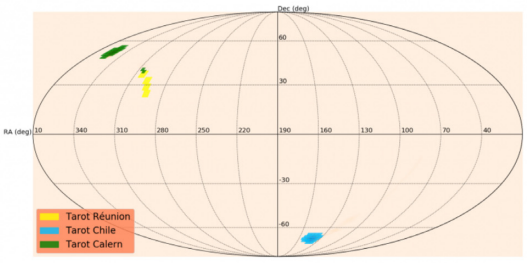

(d) S190727h

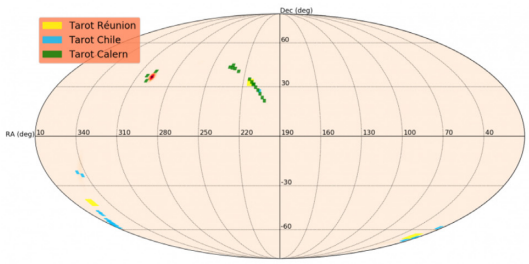

(e) S190720a

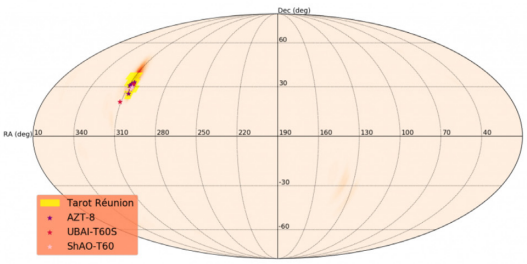

(f) S190718y

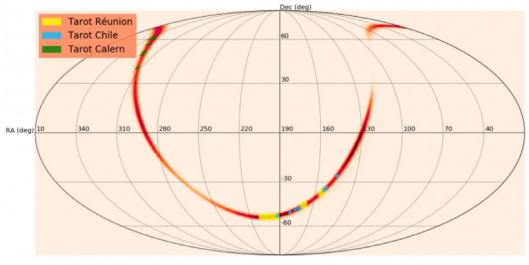

(g) S190707q

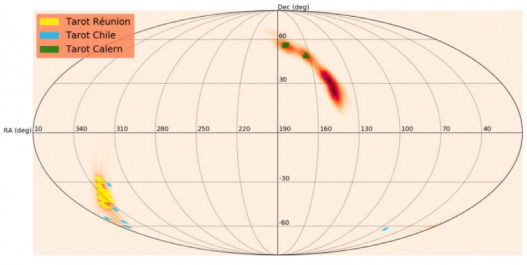

(h) S190706ai

Figure A1 – *continued*

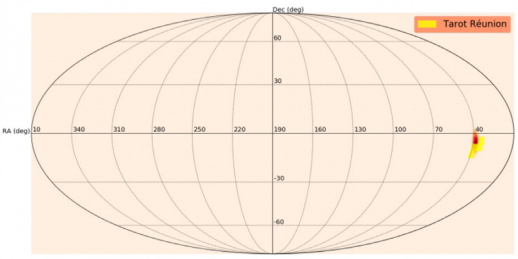

(a) S190701ah

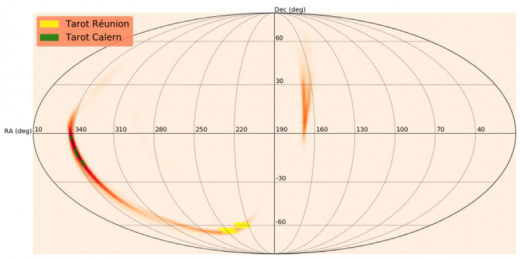

(b) S190630ag

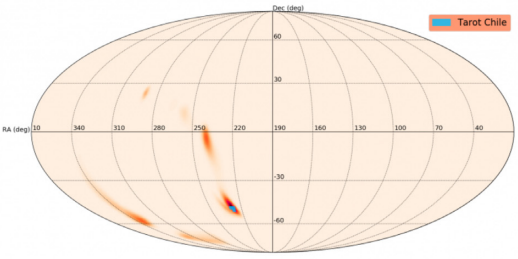

(c) S190517h

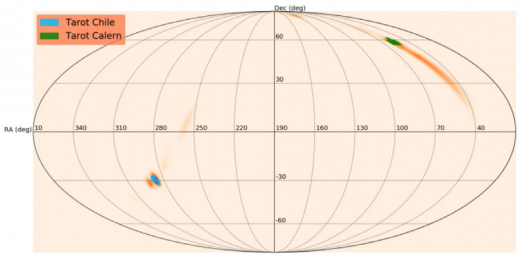

(d) S190513bm

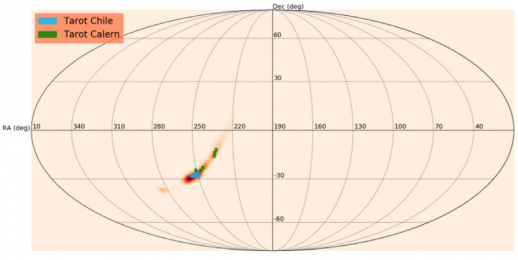

(e) S190512at

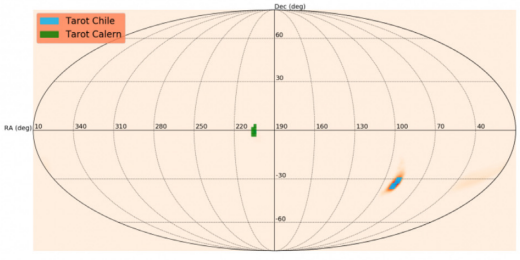

(f) S190510g

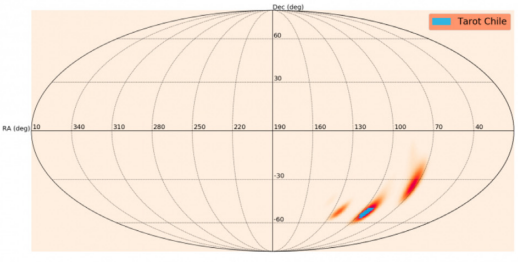

(g) S190503bf

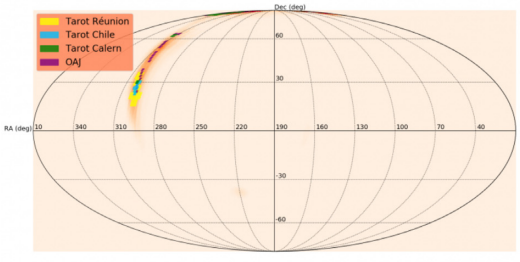

(h) S190426c

Figure A1 – *continued*

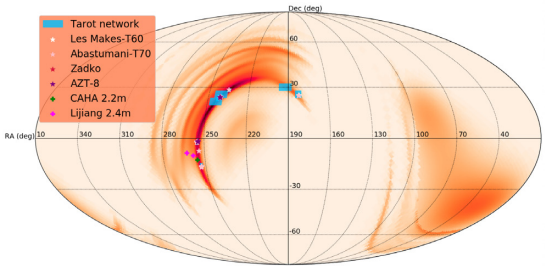

(a) S190425z

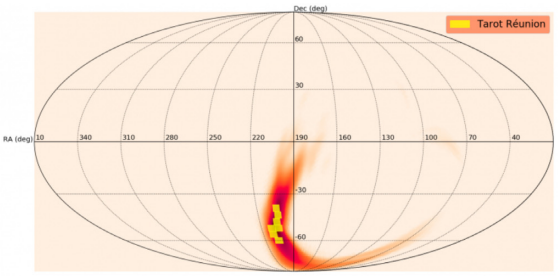

(b) S190421ar

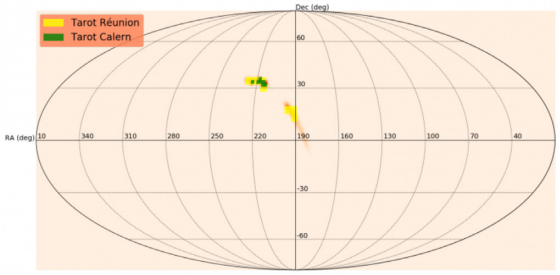

(c) S190412m

Figure A1 *–continued*

APPENDIX B: FULL OBSERVATION LOGS FOR S190425Z

Table B1. List of tiled observations performed by the TAROT network for 190425z. The probability refers to the 2D spatial probability of the LALInference GW skymap enclosed in a given tile.

Observation period (UTC)		Tile coor. (centre)		Coverage
T_{start}	T_{end}	RA [°]	Dec. [°]	prob [%]
	TAROT-TRE			
2019-04-25 14:56:19	2019-04-25 22:29:56	194.595	30.000	0.06
2019-04-25 17:03:57	2019-04-25 17:55:18	182.338	25.714	0.04
2019-04-25 17:16:58	2019-04-25 21:51:14	189.73	30.000	0.07
2019-04-25 18:07:39	2019-04-26 01:40:56	243.117	25.714	0.4
2019-04-25 18:20:49	2019-04-26 01:09:32	246.076	21.429	0.5
2019-04-25 19:11:40	2019-04-25 22:16:40	238.442	25.714	0.8
2019-04-25 19:43:51	2019-04-26 00:18:12	241.519	21.429	0.6
	TAROT-TCA			
2019-04-26 22:25:38	2019-04-28 03:32:13	255.075	−2.727	0.1
2019-04-26 22:32:16	2019-04-28 03:39:05	242.609	22.727	0.2
2019-04-26 23:18:50	2019-04-28 03:25:22	240.663	24.545	0.2
2019-04-27 19:51:10	2019-04-27 20:58:08	242.652	24.545	0.2
2019-04-27 20:44:47	2019-04-27 20:51:17	235.227	28.182	0.2
	TAROT-TCH			
2019-04-26 06:40:51	2019-04-28 01:44:47	182.983	24.545	0.01
2019-04-26 06:45:56	2019-04-28 04:51:16	235.227	28.182	0.2

Table B1 – *continued*

Observation period (UTC)		Tile coor. (centre)		Coverage
T_{start}	T_{end}	RA [°]	Dec. [°]	prob [%]
2019-04-26 06:52:44	2019-04-28 04:55:49	242.652	24.545	0.2
2019-04-26 06:59:33	2019-04-28 03:04:58	253.125	−15.455	0.1
2019-04-26 07:18:42	2019-04-27 09:38:57	242.609	22.727	0.2
2019-04-26 07:57:48	2019-04-28 05:29:50	255.075	−2.727	0.1
2019-04-27 03:18:52	2019-04-28 06:23:00	240.663	24.545	0.2

Table B2. List of galaxies, enclosed in the 3D probability region of S190425z, observed by the T60 telescope at les Makes Observatory, the T70 telescope at Abastumani Observatory, the AZT-8 telescope at Lisnyky Observatory, and the Zadko telescope.

Observation period (UTC)		Galaxy name	Galaxy coordinates		Distance
T_{start}	T_{end}		RA [°]	Dec. [°]	[Mpc]
		Les Makes/T60			
2019-04-25 15:18:10	2019-04-25 15:33:35	GWGC [MFB2005] J120819.37+251357.9	182.081	25.233	105.2
2019-04-25 15:34:40	2019-04-25 15:50:05	SDSSJ120754.97+250102.6	181.979	25.017	106.3
2019-04-25 15:34:40	2019-04-25 15:50:05	SDSSJ120754.70+250604.8	181.978	25.101	111
2019-04-25 15:34:40	2019-04-25 15:50:05	HyperLEDA 38516	182.038	25.079	111.7
2019-04-25 21:58:35	2019-04-26 00:50:20	HyperLEDA 1109773	254.435	– 1.799	136.9
2019-04-25 21:58:35	2019-04-26 00:50:20	2MASS 16574427-0147567	254.434	– 1.799	136.4
2019-04-25 21:58:35	2019-04-25 22:14:00	2MASS 16573561-0147457	254.398	– 1.796	142.6
2019-04-25 21:58:35	2019-04-25 22:14:00	HyperLEDA 1109835	254.399	– 1.796	145.1
2019-04-25 21:58:35	2019-04-25 22:14:00	2MASS 16572382-0147498	254.349	– 1.797	147.9
2019-04-25 21:58:35	2019-04-25 22:14:00	HyperLEDA 1110982	254.423	– 1.754	148.8
2019-04-25 21:58:35	2019-04-25 22:14:00	HyperLEDA 1109807	254.349	– 1.797	148.8
2019-04-25 21:58:35	2019-04-25 22:14:00	2MASS 16574141-0145157	254.423	– 1.754	168.5
2019-04-25 22:14:10	2019-04-25 22:29:35	HyperLEDA 1106076	254.456	– 1.934	136.3
2019-04-25 22:14:10	2019-04-25 22:29:35	2MASS 16574955-0156027	254.456	– 1.934	135.6
2019-04-25 22:29:45	2019-04-25 22:45:10	2MASS 16573281-0138287	254.387	– 1.641	157.3
2019-04-25 22:45:21	2019-04-25 23:00:46	2MASS 16570522-0151022	254.272	– 1.851	147.2
2019-04-25 22:45:21	2019-04-25 23:00:46	HyperLEDA 1107232	254.346	– 1.89	148.8
2019-04-25 22:45:21	2019-04-25 23:00:46	HyperLEDA 1109171	254.296	– 1.82	148.8
2019-04-25 22:45:21	2019-04-25 23:00:46	2MASS 16572303-0153258	254.346	– 1.891	155.8
2019-04-25 22:45:21	2019-04-25 23:00:46	2MASS 16571094-0149128	254.296	– 1.82	169.9
2019-04-25 23:00:56	2019-04-26 00:50:20	2MASS 16580368-0150074	254.515	– 1.835	147.5
2019-04-25 23:00:56	2019-04-25 23:16:21	HyperLEDA 1108643	254.598	– 1.839	136.9
2019-04-25 23:00:56	2019-04-26 00:50:20	2MASS 16580515-0149544	254.521	– 1.832	162.3
2019-04-25 23:16:31	2019-04-25 23:31:56	2MASS 16585823-0202277	254.743	– 2.041	132.1
2019-04-25 23:16:31	2019-04-25 23:31:56	HyperLEDA 161011	254.743	– 2.041	145
2019-04-25 23:16:31	2019-04-25 23:31:56	HyperLEDA 161014	254.822	– 2.074	120.5
2019-04-25 23:16:31	2019-04-25 23:31:56	2MASS 16591729-0204281	254.822	– 2.074	107.3
2019-04-25 23:32:06	2019-04-25 23:47:31	HyperLEDA 161013	254.775	– 1.914	133.6
2019-04-25 23:32:06	2019-04-25 23:47:31	2MASS 16592042-0153111	254.835	– 1.886	147
2019-04-25 23:32:06	2019-04-25 23:47:31	HyperLEDA 161015	254.835	– 1.886	148.1
2019-04-25 23:32:06	2019-04-25 23:47:31	2MASS 16590588-0154501	254.775	– 1.914	128.1
2019-04-25 23:47:49	2019-04-26 00:03:14	6dFJ1654221-164837	253.592	– 16.81	122.3
2019-04-25 23:47:49	2019-04-26 00:03:14	2MASS 16542215-1648370	253.592	– 16.81	122.5
2019-04-26 00:03:31	2019-04-26 00:18:56	HyperLEDA 1093975	255.095	– 2.372	140.4
2019-04-26 00:03:31	2019-04-26 00:18:56	HyperLEDA 161019	255.096	– 2.326	143.6
2019-04-26 00:03:31	2019-04-26 00:18:56	HyperLEDA 1092764	255.06	– 2.413	145
2019-04-26 00:03:31	2019-04-26 00:18:56	2MASS 17002062-0225482	255.086	– 2.43	145.6
2019-04-26 00:03:31	2019-04-26 00:18:56	2MASS 17002302-0219322	255.096	– 2.326	129
2019-04-26 00:03:31	2019-04-26 00:18:56	2MASS 17001441-0224462	255.06	– 2.413	147.4
2019-04-26 00:03:31	2019-04-26 00:18:56	2MASS 17002095-0217192	255.087	– 2.289	151.5
2019-04-26 00:03:31	2019-04-26 00:18:56	2MASS 17002288-0222202	255.095	– 2.372	120.1
2019-04-26 00:19:13	2019-04-26 00:34:38	HyperLEDA 899699	253.301	– 16.316	118.8
2019-04-26 00:19:13	2019-04-26 00:34:38	HyperLEDA 899284	253.355	– 16.349	118.8
2019-04-26 00:19:13	2019-04-26 00:34:38	HyperLEDA 900018	253.27	– 16.291	122.8
2019-04-26 00:19:13	2019-04-26 00:34:38	2MASS 16530485-1617273	253.27	– 16.291	123
2019-04-26 00:19:13	2019-04-26 00:34:38	2MASS 16532193-1617132	253.341	– 16.287	129.8
2019-04-26 00:19:13	2019-04-26 00:34:38	2MASS 16531513-1621223	253.313	– 16.356	99.7
2019-04-26 00:34:55	2019-04-26 00:50:20	HyperLEDA 1109100	254.506	– 1.823	138

Table B2 – *continued*

Observation period (UTC)		Galaxy name	Galaxy coordinates		Distance
T_{start}	T_{end}		RA [°]	Dec. [°]	[Mpc]
2019-04-26 00:34:55	2019-04-26 00:50:20	2MASS 16580128-0149216	254.505	– 1.823	136.4
2019-04-26 00:50:34	2019-04-26 01:05:59	HyperLEDA 161003	253.86	– 7.206	132.3
2019-04-26 00:50:34	2019-04-26 01:05:59	2MASS 16552449-0715255	253.852	– 7.257	130.1
2019-04-26 00:50:34	2019-04-26 01:05:59	HyperLEDA 161002	253.852	– 7.257	130.7
		Abastumani/T70			
2019-04-25 23:08:01	2019-04-25 23:15:13	GWGC UGC07124	182.193	24.946	100.5
2019-04-25 23:08:01	2019-04-25 23:15:13	GWGC PGC038615	182.325	24.968	102.7
2019-04-25 23:08:01	2019-04-25 23:15:13	GWGC PGC038526	182.055	24.943	105.7
2019-04-25 23:22:46	2019-04-25 23:29:58	HyperLEDA 1093975	255.095	– 2.372 140.4	
2019-04-25 23:22:46	2019-04-25 23:29:58	HyperLEDA 161019	255.096	– 2.326	143.6
2019-04-25 23:22:46	2019-04-25 23:29:58	HyperLEDA 1092764	255.06	– 2.413	145
2019-04-25 23:22:46	2019-04-25 23:29:58	2MASS 17002062-0225482	255.086	– 2.43	145.6
2019-04-25 23:22:46	2019-04-25 23:29:58	2MASS 17002302-0219322	255.096	– 2.326	129
2019-04-25 23:22:46	2019-04-25 23:29:58	2MASS 17001441-0224462	255.06	– 2.413	147.4
2019-04-25 23:22:46	2019-04-25 23:29:58	2MASS 17002095-0217192	255.087	– 2.289	151.5
2019-04-25 23:22:46	2019-04-25 23:29:58	2MASS 17002288-0222202	255.095	– 2.372	120.1
2019-04-25 23:37:08	2019-04-25 23:44:20	HyperLEDA 899699	253.301	– 16.316	118.8
2019-04-25 23:37:08	2019-04-25 23:44:20	HyperLEDA 899284	253.355	– 16.349	118.8
2019-04-25 23:37:08	2019-04-25 23:44:20	HyperLEDA 900018	253.27	– 16.291	122.8
2019-04-25 23:37:08	2019-04-25 23:44:20	2MASS 16530485-1617273	253.27	– 16.291	123
2019-04-25 23:37:08	2019-04-25 23:44:20	2MASS 16532193-1617132	253.341	– 16.287	129.8
2019-04-25 23:37:08	2019-04-25 23:44:20	2MASS 16531513-1621223	253.313	– 16.356	99.7
2019-04-25 23:54:01	2019-04-26 00:01:13	6dFJ1653567-160711	253.486	– 16.12	121.9
2019-04-25 23:54:01	2019-04-26 00:01:13	2MASS 16535674-1607110	253.486	– 16.12	122.1
2019-04-25 23:54:01	2019-04-26 00:01:13	2MASS 16535385-1614537	253.474	– 16.248	109.3
2019-04-26 00:04:49	2019-04-26 00:12:01	HyperLEDA 896696	253.494	– 16.552	121.4
2019-04-26 00:17:30	2019-04-26 00:24:42	2MASS 17005715-0225086	255.238	– 2.419	127
2019-04-26 00:17:30	2019-04-26 00:24:42	2MASS 17012357-0220366	255.348	– 2.344	146.1
2019-04-26 00:17:30	2019-04-26 00:24:42	HyperLEDA 1094718	255.348	– 2.344	150.5
2019-04-26 00:30:30	2019-04-26 00:37:42	HyperLEDA 1697461	241.489	23.986	148.8
2019-04-26 00:30:30	2019-04-26 00:37:42	HyperLEDA 1696139	241.357	23.92	136.9
2019-04-26 00:42:34	2019-04-26 00:49:45	SDSSJ154308.15+282509.9	235.784	28.419	145
2019-04-26 00:42:34	2019-04-26 00:49:45	HyperLEDA 1835553	235.651	28.432	143.7
2019-04-26 00:55:56	2019-04-26 01:03:07	HyperLEDA 1697264	240.942	23.977	157.7
2019-04-26 00:55:56	2019-04-26 01:03:07	HyperLEDA 1695306	240.892	23.875	153.6
2019-04-26 00:55:56	2019-04-26 01:03:07	HyperLEDA 56887	240.925	24.095	140.9
2019-04-26 01:09:56	2019-04-26 01:17:08	HyperLEDA 56963	241.153	23.663	165.5
2019-04-26 01:09:56	2019-04-26 01:17:08	HyperLEDA 1691288	241.25	23.658	166.8
2019-04-26 01:09:56	2019-04-26 01:17:08	HyperLEDA 1693165	241.235	23.758	170.6
2019-04-26 01:09:56	2019-04-26 01:17:08	HyperLEDA 1690684	241.15	23.625	163.5
2019-04-26 01:09:56	2019-04-26 01:17:08	HyperLEDA 57021	241.26	23.669	146.9
2019-04-26 01:09:56	2019-04-26 01:17:08	HyperLEDA 1690441	241.184	23.612	151.4
2019-04-26 01:21:42	2019-04-26 01:28:54	SDSSJ160409.58+241950.7	241.04	24.331	168.7
2019-04-26 01:21:42	2019-04-26 01:28:54	HyperLEDA 1706506	240.988	24.402	169.4
2019-04-26 01:21:42	2019-04-26 01:28:54	HyperLEDA 1706072	241.077	24.382	151.9
2019-04-26 01:21:42	2019-04-26 01:28:54	HyperLEDA 1703751	241.076	24.281	147.3
		Lisnyky/AZT-8			
2019-04-25 22:32:38	2019-04-25 22:56:24	HyperLEDA 1107232	254.346	– 1.89	148.8
2019-04-25 22:32:38	2019-04-25 22:56:24	2MASS 16572303-0153258	254.346	– 1.891	155.8
2019-04-25 23:01:18	2019-04-25 23:21:22	2MASS 16570522-0151022	254.272	– 1.851	147.2
2019-04-25 23:01:18	2019-04-25 23:21:22	HyperLEDA 1109171	254.296	– 1.82	148.8
2019-04-25 23:01:18	2019-04-25 23:21:22	2MASS 16571094-0149128	254.296	– 1.82	169.9
2019-04-25 23:24:57	2019-04-25 23:45:08	HyperLEDA 1109773	254.435	– 1.799	136.9
2019-04-25 23:24:57	2019-04-25 23:45:08	2MASS 16574427-0147567	254.434	– 1.799	136.4
2019-04-25 23:24:57	2019-04-25 23:45:08	2MASS 16573561-0147457	254.398	– 1.796	142.6
2019-04-25 23:24:57	2019-04-25 23:45:08	HyperLEDA 1109835	254.399	– 1.796	145.1
2019-04-25 23:24:57	2019-04-25 23:45:08	2MASS 16572382-0147498	254.349	– 1.797	147.9
2019-04-25 23:24:57	2019-04-25 23:45:08	HyperLEDA 1110982	254.423	– 1.754	148.8
2019-04-25 23:24:57	2019-04-25 23:45:08	HyperLEDA 1109807	254.349	– 1.797	148.8
2019-04-25 23:24:57	2019-04-25 23:45:08	2MASS 16574141-0145157	254.423	– 1.754	168.5
2019-04-25 23:56:12	2019-04-26 00:16:25	HyperLEDA 1699170	241.231	24.073	165.3
2019-04-25 23:56:12	2019-04-26 00:16:25	SDSSJ160504.21+240240.4	241.268	24.045	154.1

Table B2 – *continued*

Observation period (UTC)		Galaxy name	Galaxy coordinates		Distance
T_{start}	T_{end}		RA [°]	Dec. [°]	[Mpc]
2019-04-26 00:17:33	2019-04-26 00:37:36	HyperLEDA 140564	241.215	23.938	161.5
2019-04-26 00:17:33	2019-04-26 00:37:36	HyperLEDA 1695387	241.253	23.879	154.2
2019-04-26 00:17:33	2019-04-26 00:37:36	SDSSJ160454.83+235507.5	241.229	23.919	146
2019-04-26 00:17:33	2019-04-26 00:37:36	HyperLEDA 57003	241.211	23.975	176.2
2019-04-26 00:17:33	2019-04-26 00:37:36	HyperLEDA NGC 6051	241.236	23.933	143.6
2019-04-26 00:17:33	2019-04-26 00:37:36	HyperLEDA 57014	241.248	23.97	140.2
2019-04-26 00:40:37	2019-04-26 01:01:06	HyperLEDA 1697461	241.489	23.986	148.8
2019-04-26 01:03:45	2019-04-26 01:24:03	SDSSJ160519.85+235455.0	241.333	23.915	149.7
2019-04-26 01:03:45	2019-04-26 01:24:03	SDSSJ160505.95+235227.2	241.275	23.874	175.9
2019-04-26 01:03:45	2019-04-26 01:24:03	SDSSJ160512.22+235109.2	241.301	23.853	136.9
2019-04-26 01:03:45	2019-04-26 01:24:03	HyperLEDA 1696139	241.357	23.92	136.9
		Zadko			
2019-04-25 14:56:19	2019-04-26 19:00:00	2MASS 16580128-0149216	254.505	– 1.822	136.4
2019-04-25 14:56:19	2019-04-26 19:00:00	2MASS 16574955-0156027	254.456	– 1.934	135.6
2019-04-25 14:56:19	2019-04-26 19:00:00	2MASS 16572303-0153258	254.345	– 1.890	155.8
2019-04-25 14:56:19	2019-04-26 19:00:00	2MASS 16580515-0149544	254.521	– 1.831	162.3
2019-04-25 14:56:19	2019-04-26 19:00:00	2MASS 16580368-0150074	254.515	– 1.835	147.4
2019-04-25 14:56:19	2019-04-26 19:00:00	2MASS 16582363-0154183	254.598	– 1.905	186.2
2019-04-25 14:56:19	2019-04-26 19:00:00	2MASS 16574594-0148107	254.441	– 1.802	182.0
2019-04-25 14:56:19	2019-04-26 19:00:00	2MASS 16575261-0148017	254.469	– 1.800	188.5
2019-04-25 14:56:19	2019-04-26 19:00:00	HyperLEDA 1106076	254.456	– 1.934	136.3
2019-04-25 14:56:19	2019-04-26 19:00:00	HyperLEDA 1107232	254.346	– 1.890	148.8
2019-04-25 14:56:19	2019-04-26 19:00:00	HyperLEDA 1109100	254.506	– 1.822	138.0
2019-04-25 14:56:19	2019-04-26 19:00:00	2MASS 16580128-0149216	254.505	– 1.822	136.4
2019-04-25 14:56:19	2019-04-26 19:00:00	2MASS 16574427-0147567	254.434	– 1.799	136.4
2019-04-25 14:56:19	2019-04-26 19:00:00	2MASS 16574955-0156027	254.456	– 1.934	135.6
2019-04-25 14:56:19	2019-04-26 19:00:00	2MASS 16573561-0147457	254.398	– 1.796	142.6
2019-04-25 14:56:19	2019-04-26 19:00:00	2MASS 16572382-0147498	254.349	– 1.797	147.9
2019-04-25 14:56:19	2019-04-26 19:00:00	2MASS 16571094-0149128	254.295	– 1.820	169.9
2019-04-25 14:56:19	2019-04-26 19:00:00	2MASS 16572303-0153258	254.345	– 1.890	155.8
2019-04-25 14:56:19	2019-04-26 19:00:00	2MASS 16580515-0149544	254.521	– 1.831	162.3
2019-04-25 14:56:19	2019-04-26 19:00:00	2MASS 16580368-0150074	254.515	– 1.835	147.5
2019-04-25 14:56:19	2019-04-26 19:00:00	2MASS 16580581-0143094	254.524	– 1.719	113.5
2019-04-25 14:56:19	2019-04-26 19:00:00	2MASS 16575321-0141247	254.471	– 1.690	174.9
2019-04-25 14:56:19	2019-04-26 19:00:00	2MASS 16574141-0145157	254.422	– 1.754	168.5
2019-04-25 14:56:19	2019-04-26 19:00:00	2MASS 16574594-0148107	254.441	– 1.802	182.0
2019-04-25 14:56:19	2019-04-26 19:00:00	2MASS 16575261-0148017	254.469	– 1.800	188.5
2019-04-25 14:56:19	2019-04-26 19:00:00	2MASS 16575048-0145247	254.460	– 1.756	185.9
2019-04-25 14:56:19	2019-04-26 19:00:00	2MASS 16570522-0151022	254.271	– 1.850	147.2
2019-04-25 14:56:19	2019-04-26 19:00:00	HyperLEDA 1106076	254.456	– 1.934	136.3
2019-04-25 14:56:19	2019-04-26 19:00:00	HyperLEDA 1107232	254.346	– 1.890	148.8
2019-04-25 14:56:19	2019-04-26 19:00:00	HyperLEDA 1109100	254.506	– 1.822	138.0
2019-04-25 14:56:19	2019-04-26 19:00:00	HyperLEDA 1109171	254.296	– 1.820	148.8
2019-04-25 14:56:19	2019-04-26 19:00:00	HyperLEDA 1109773	254.435	– 1.799	136.9
2019-04-25 14:56:19	2019-04-26 19:00:00	HyperLEDA 1109807	254.349	– 1.797	148.8
2019-04-25 14:56:19	2019-04-26 19:00:00	HyperLEDA 1109835	254.399	– 1.796	145.1
2019-04-25 14:56:19	2019-04-26 19:00:00	HyperLEDA 1110982	254.423	– 1.754	148.8
2019-04-25 14:56:19	2019-04-26 19:00:00	2MASS 16573561-0147457	254.398	– 1.796	142.6
2019-04-25 14:56:19	2019-04-26 19:00:00	2MASS 16572382-0147498	254.349	– 1.797	147.9
2019-04-25 14:56:19	2019-04-26 19:00:00	2MASS 16564648-0157432 1105380	254.193	– 1.962	149.8
2019-04-25 14:56:19	2019-04-26 19:00:00	2MASS 16571094-0149128	254.295	– 1.820	169.9
2019-04-25 14:56:19	2019-04-26 19:00:00	2MASS 16572303-0153258	254.345	– 1.890	155.8
2019-04-25 14:56:19	2019-04-26 19:00:00	2MASS 16570522-0151022	254.271	– 1.850	147.2
2019-04-25 14:56:19	2019-04-26 19:00:00	HyperLEDA 1107232	254.346	– 1.890	148.8
2019-04-25 14:56:19	2019-04-26 19:00:00	HyperLEDA 1109171	254.296	– 1.820	148.8
2019-04-25 14:56:19	2019-04-26 19:00:00	HyperLEDA 1109807	254.349	– 1.797	148.8
2019-04-25 14:56:19	2019-04-26 19:00:00	HyperLEDA 1109835	254.399	– 1.796	145.1
2019-04-25 14:56:19	2019-04-26 19:00:00	2MASS 16045670+2355583 NGC 6051	241.236	23.932	143.6
2019-04-25 14:56:19	2019-04-26 19:00:00	2MASS 16045057+2358303 57003	241.210	23.975	176.2
2019-04-25 14:56:19	2019-04-26 19:00:00	2MASS 16045947+2358123 57014	241.247	23.970	140.2
2019-04-25 14:56:19	2019-04-26 19:00:00	2MASS 16043249+2356393 140561	241.135	23.944	148.2
2019-04-25 14:56:19	2019-04-26 19:00:00	2MASS 16045152+2356153 140564	241.214	23.937	161.5
2019-04-25 14:56:19	2019-04-26 19:00:00	HyperLEDA 1699170	241.231	24.073	165.3

Table B2 – *continued*

Observation period (UTC)		Galaxy name	Galaxy coordinates		Distance
T_{start}	T_{end}		RA [°]	Dec. [°]	[Mpc]
2019-04-25 14:56:19	2019-04-26 19:00:00	SDSSJ160504.21+240240.4	241.268	24.044	154.1
2019-04-25 14:56:19	2019-04-26 19:00:00	SDSSJ160427.52+240639.8	241.115	24.111	151.2
2019-04-25 14:56:19	2019-04-26 19:00:00	SDSSJ160454.83+235507.5	241.229	23.918	146.0
2019-04-25 14:56:19	2019-04-26 19:00:00	2MASS 16045670+2355583 NGC 6051	241.236	23.932	143.6
2019-04-25 14:56:19	2019-04-26 19:00:00	2MASS 16050427+2355015 57025	241.267	23.917	237.2
2019-04-25 14:56:19	2019-04-26 19:00:00	2MASS 16043346+2350163 56958	241.139	23.837	185.2
2019-04-25 14:56:19	2019-04-26 19:00:00	2MASS 16045057+2358303 57003	241.210	23.975	176.2
2019-04-25 14:56:19	2019-04-26 19:00:00	2MASS 16045947+2358123 57014	241.247	23.970	140.2
2019-04-25 14:56:19	2019-04-26 19:00:00	2MASS 16043249+2356393 140561	241.135	23.944	148.2
2019-04-25 14:56:19	2019-04-26 19:00:00	2MASS 16045152+2356153 140564	241.214	23.937	161.5
2019-04-25 14:56:19	2019-04-26 19:00:00	HyperLEDA 1695387	241.253	23.879	154.2
2019-04-25 14:56:19	2019-04-26 19:00:00	SDSSJ160454.83+235507.5	241.229	23.918	146.0
2019-04-25 14:56:19	2019-04-26 19:00:00	SDSSJ160505.95+235227.2	241.275	23.874	175.9

[1]*APC, Univ. Paris Diderot, CNRS/IN2P3, CEA/lrfu, Obs de Paris, Sorbonne, 75013 Paris Cité, France*
[2]*N.Tusi Shamakhy Astrophysical Observatory, Azerbaijan National Academy of Sciences, settl.Mamedaliyev, AZ 5626 Shamakhy, Azerbaijan*
[3]*E.Kharadze Abastumani Astrophysical Observatory Mt.Kanobili, Ilia State University, Abastumani, 0301 Adigeni, Georgia*
[4]*Samtskhe-Javakheti State University, Rustaveli Str. 113, Akhaltsikhe 0080, Georgia*
[5]*UPMC-CNRS, UMR7095, Institut d'Astrophysique de Paris, F-75014 Paris, France*
[6]*Astronomical Observatory, Taras Shevshenko National University of Kyiv, Observatorna str. 3, Kyiv UA-04053, Ukraine*
[7]*Nuclear Physics Department, Taras Shevchenko National University of Kyiv, 60 Volodymyrska str., Kyiv UA-01601, Ukraine*
[8]*Yunnan Astronomical Observatories/Chinese Academy of Science, Kunming 650011, China*
[9]*Laboratoire d'Astrophysique de Marseille, UMR 7326, CNRS, Université d'Aix Marseille, 38, rue Frédéric Joliot-Curie,Marseille, France*
[10]*AGORA Observatoire des Makes, AGORA, 18 Rue Georges Bizet, Observatoire des Makes, F-97421 La Rivière, France*
[11]*Instituto de Astrofísica de Andalucía (IAA-CSIC), Glorieta de la Astronomía s/n, E-18008 Granada, Spain*
[12]*ARTEMIS UMR 7250 UCA CNRS OCA, Boulevard de l'Observatoire, CS 34229, 06304 Nice CEDEX 04, France*
[13]*Ulugh Beg Astronomical Institute, Uzbekistan Academy of Sciences, Astronomy str. 33, Tashkent 100052, Uzbekistan*
[14]*OzGrav-UWA, University of Western Australia, School of Physics, M013, 35 Stirling Highway, Crawley, WA 6009, Australia*
[15]*IRAP, Université de Toulouse, CNRS, UPS, 14 Avenue Edouard Belin, F-31400 Toulouse, France*
[16]*Université Paul Sabatier Toulouse III, Université de Toulouse, 118 Route de Narbonne, F-31400 Toulouse, France*
[17]*WuZhou University, Wuzhou, Guangxi 543000, China*
[18]*AIM, CEA, CNRS, Université Paris-Saclay, Université Paris Diderot, Sorbonne Paris Cité, F-91191 Gif-sur-Yvette, France*
[19]*LAL, Univ Paris-Sud, CNRS/IN2P3, Orsay, France*
[20]*California Institute of Technology, 1200 East California Blvd, MC 249-17, Pasadena, CA 91125, USA*
[21]*Nikhef, Science Park, NL-1098 XG Amsterdam, the Netherlands*
[22]*National Astronomical Observatories/Chinese Academy of Science 20A Datun Road, Beijing 100012, China*
[23]*Physics Department and Astronomy Department, Tsinghua University, Beijing 100084, China*
[24]*Astronomy and Space Physics Department, Taras Shevchenko National University of Kyiv, 60 Volodymyrska str., Kyiv UA-01601, Ukraine*

This paper has been typeset from a TEX/LATEX file prepared by the author.